coatings

MDPI

Article

Short- and Long-Term Electrochemical Response Prediction of Ni-Al-Powder-Coated Steel with Machine Learning

Ayla Ocak [1], Ümit Işıkdağ [2], Sinan Melih Nigdeli [3,*] and Gebrail Bekdaş [3,*]

[1] Smart Infrastructure Technician Program, Gelisim Vocational School, Istanbul Gelisim University, Istanbul 34310, Türkiye; ayocak@gelisim.edu.tr
[2] Department of Architecture, Mimar Sinan Fine Arts University, Istanbul 34427, Türkiye; umit.isikdag@msgsu.edu.tr
[3] Department of Civil Engineering, İstanbul University-Cerrahpaşa, Istanbul 34320, Türkiye
* Correspondence: melihnig@iuc.edu.tr (S.M.N.); bekdas@iuc.edu.tr (G.B.)

Highlights

What are the main findings?

- Random forest accurately predicted EIS Bode responses of coated steel.
- Short- and long-term impedance and phase angles were predicted.
- Multi-seed analysis confirmed model stability and reproducibility.

What are the implications of the main findings?

- ML can reduce costly and time-consuming corrosion experiments.
- The method enables rapid corrosion assessment of Ni-Al coatings.
- The framework supports AI-assisted coating performance evaluation.

Abstract

Steel is the most fundamental material used in structural system elements in the construction industry. It needs to be coated with materials that provide resistance to high temperatures, wear, and corrosion. Ni-Al powder is preferred in coatings because nickel increases corrosion resistance and aluminium forms an oxide layer to reduce oxidation. In the long term, the protective effect of coatings decreases, and corrosion resistance declines. In this study, a random forest model was evaluated using experimental data on the corrosion performance of A36 steel coated with Ni-Al powder for corrosion prevention, after exposure to a 3.5% NaCl solution for 1 h and 30 days for short- and long-term electrochemical response prediction. The impedance and phase angle characteristics, which represent the electrochemical response of coated and uncoated steel, have been predicted. In addition, the model's reproducibility was investigated using the multi-seed (30 seeds) method to analyse the stability and consistency of the random forest model. The aim of this study was to develop a machine learning model that learns the frequency-dependent electrochemical impedance (Bode) response of graphene oxide-enriched Ni–Al coatings on steel, which reflects the corrosion-related electrochemical behaviour of the coating system, and to evaluate the model for predicting the impedance magnitude and phase angle of reference coatings over the investigated frequency range. The developed artificial intelligence model predicted the Bode response (impedance magnitude and phase angle) of coated and uncoated steel to NaCl solution after 1 h and 30 days as a function of frequency and coating type. The predicted impedance spectra reflected the deterioration of the corrosion protection performance of the Ni–Al coatings with increasing exposure time. The predicted EIS responses were subsequently used to assess changes in the corrosion-related electrochemical behaviour of the coatings over short- and long-term exposure. According to the

Academic Editors: Binbin Zhang and Alexander Tolstoguzov

Received: 10 July 2026
Revised: 3 August 2026
Accepted: 4 August 2026
Published: 6 August 2026

findings, the random forest models can predict the frequency-dependent electrochemical response (impedance magnitude and phase angle) with high accuracy.

Keywords: electrochemical response; coated steel; corrosion resistance; artificial intelligence; machine learning; prediction

1. Introduction

Steel is a preferred structural material in the design of reinforced concrete and steel structures due to the strength it adds to the structure. Its main areas of use in structural systems are load-bearing system elements, roof systems, bridges, prefabricated structures, industrial buildings, towers and poles, large-span structures, and facade systems. In addition to enabling column-free spanning of wide openings, it offers ease of rapid production and assembly. By providing strength to the structure and resisting vibrations, it contributes to the safety and longevity of bridge projects such as highways and railways. It is advantageous for electrical transmission lines and telecommunication towers that require wind resistance and safe transport of equipment. It is suitable for strengthening structures and stands out for its ease of maintenance when a damaged part occurs. The basic building blocks of steel are iron and carbon. The carbon content determines the hardness of the steel and affects its brittleness. In addition to these components, the properties of steel can be improved by adding elements such as chromium, vanadium, manganese, etc. The addition of vanadium can increase the hardness of steel [1]. High manganese content gives steel high strength, wear resistance, ductility, toughness and excellent strain hardening properties [2–4]. Chromium, on the other hand, is used to balance the corrosion resistance of steel. Chromium alloy steels have been developed to improve the corrosion resistance of steel by using chromium alloys in different proportions. Studies support the fact that steels with a chromium alloy content of around 3%–5% significantly reduce the corrosion rate and are effective in preventing localised corrosion that may develop in a CO_2 environment [5–9].

Steel is a product susceptible to environmental factors. Structures such as roof systems, offshore platforms, floating piers, submarine pipelines, and transmission towers are particularly exposed to various natural sources like rainwater and saltwater. This exposure causes corrosion of the steel structure, leading to a decrease in its durability and damage due to wear. Steel used in marine structures, in particular, is exposed to high amounts of chloride ions, causing wear and corrosion. To prevent this, various methods have been tried for steel, and coatings that delay or minimise corrosion have been investigated. The basic principle applied in ensuring the corrosion resistance of steel is to restrict water access and prevent oxygen from reaching the steel. Corrosion prevention measures are taken in two ways: active and passive protection. In active corrosion protection, chemicals (inhibitors) are used to create an absorbed film layer on the surface of the metal, or the inhibitors interact with the corrosion-causing component to reduce corrosion [10,11]. In passive protection, corrosion is prevented by constructing an oxide barrier between the coating and the metal surface [10,12]. Chromium is effective in the corrosion resistance of steel and is preferred in steel coatings. However, after the carcinogenic effect of hexavalent chromium was discovered in the 1990s, it was banned in various countries (since 2006), and efforts were made to reduce the use of chromium coatings [13,14]. As an alternative coating, thin organic coatings, consisting of a polymer-containing acrylic film layer that provides a good metallic appearance and supports wear resistance, have been used [13]. Although organic coatings act as a barrier between the metal surface and the environment that can cause corrosion, they are affected by various environmental conditions in the long term, and the protective wall weakens. Examples of these include pH value, electrolyte flow rate, temperature, and dissolved oxygen [15–21]. It has been stated that increasing the flow rate increases the corrosion rate of steel in the case of low CO_2 partial pressure [16,22,23]. In addition, the pH of the solution to which the steel is exposed significantly affects the polarity change and thus the corrosion of the material [18]. High temperatures accelerate and increase the severity of corrosion deterioration [19]. Increasing the dissolved oxygen content accelerates cathodic corrosion, increases passive film formation and polarisation resistance [24]. Another type of coating used to protect steel against corrosion is composite coatings. Composite coatings are a type of coating consisting of a base body (matrix material) of the coating, which is mostly metallic, and reinforcement materials added to the body. It consists of two phases: matrix phase and reinforcement phase. The matrix material is the main component responsible for holding the reinforced materials together for the composite [25]. Reinforcement materials are known as materials that affect the adhesion performance and corrosion resistance of the composite coating to the steel surface. In composite coatings used for corrosion resistance of steel, matrix materials such as aluminium (Al) [26], zinc oxide (ZnO) [27], nickel (Ni) [28,29], zinc (Zn) [30], tin (Sn) [31], and nickel phosphorus (Ni-P) [32–34] are used, while reinforcement materials such as silicon carbide (SiC) [28,29], alumina (Al_2O_3) [28,29], zirconium dioxide (ZrO_2) [28], tungsten carbide (WC) [28], graphene [30,31,35], titanium dioxide (TiO_2) [28,32,34] and carbon nanotube (CNT) are preferred. Nickel-based composites are frequently preferred in coatings due to their good hardness and effectiveness in preventing corrosion [36,37]. As a second-phase material, many products have been tested on nickel-based coatings, and graphene oxide materials obtained by oxidation of graphene and graphite have stood out with their electrical and mechanical responses to corrosion. Graphene has been evaluated as a composite coating against corrosion in its pure form or in metallic coatings [30,31,37–40]. It is a material with good electrical [30] and thermal conductivity [30,41], high mechanical strength [42,43] and impermeability in corrosive environments [37,42]. Graphene oxide (GO), as a derivative of graphene, is one of the alternative second-phase materials to graphene. Unlike graphene, which exhibits hydrophobic properties, it exhibits hydrophilic properties due to the oxygen it contains and disperses easily in water [37,39,44,45]. Several studies support the fact that the use of graphene oxide as a second phase in nickel-based composite coatings applied to steel significantly reduces corrosion by increasing friction and wear resistance [46–48]. The common GO effect in the research is associated with the impermeability of graphene, its distribution in the nickel-based matrix material, its stable structure, and the reduction in grain size [49]. In nickel-based composites, aluminium elements and their compounds can be evaluated together. In coatings rich in aluminium content, resistance to high temperatures increases. Al-containing alloys provide thermal stability to the coating [50]. By adding aluminium to nickel coatings, a corrosion-resistant composite with good hardness and resistance to high temperatures can be obtained. Various techniques such as electrodeposition [51,52], chemical or physical vapour deposition [53,54], and plasma spraying [55,56] are applied in the application of coatings. In the plasma spraying method, the coating, melted in a high-temperature plasma jet, adheres well to substrates such as steel. In plasma spraying of coatings containing Ni-Al and using GO filler, Ni-Al powder is melted in a high-temperature plasma jet and transported to the coating surface, and the hydrophilic property of graphene oxide contributes to a more homogeneous distribution.

Artificial intelligence is a computational method that learns from available data and makes inferences based on the information it acquires. In the coating of metals against corrosion, artificial intelligence technologies can be used to predict the properties of coating materials that are effective in reducing corrosion rates. With machine learning techniques, i.e., a subfield of artificial intelligence, correlations between variables can be determined by evaluating multiple parameters together, instead of analyses based on two parameters [57,58]. In this way, the effect of multiple properties that are effective in the coating on the performance of the coating can be evaluated simultaneously. With artificial intelligence techniques, highly accurate predictions can be made based on available data by reducing experimental procedures that require time and cost. Remarkable results can be obtained in areas such as determining coating performance and predicting mechanical properties.

In this study, the frequency-dependent electrochemical impedance spectroscopy (EIS) response (Bode response) of a composite coating using graphene oxide reinforcement with Ni-Al matrix material was predicted using machine learning (ML). The predicted EIS response was subsequently used to assess the corrosion-related electrochemical behaviour of the coating system. For this purpose, using the experimental results of A36 steel coated with Ni-Al powder and graphene oxide by the plasma spraying method [56], ML models were developed to predict the short- and long-term Bode response (the electrochemical response after 1 h and 30 days of exposure to a 3.5% NaCl solution). The predicted Bode response reflects the corrosion-related electrochemical behaviour of the coating system. Information on prediction applications with artificial intelligence techniques in the literature on coatings is presented in the next section.

2. Literature Review: Prediction of Corrosion-Related Electrochemical Responses in Coatings

The number of factors affecting the corrosion resistance of coatings is quite large. These factors include the porosity of the coating, the adhesion between the substrate and the coating, the coating density, thickness, water/moisture or ion permeability, homogeneous distribution, and environmental conditions. Furthermore, the hardness of the coating can also affect corrosion resistance by making it difficult for water/moisture, oxygen, or Cl^- ions to pass through the coated metal. The electrochemical response of coatings is important in evaluating their corrosion performance. Various tests and analyses, such as potentiodynamic polarisation testing, electrochemical impedance spectroscopy (EIS), and open-circuit potential (OCP), are performed to measure the electrochemical response of the coating [59].

As a result of analyses conducted on the corrosion performance of the coating, EIS data such as impedance and phase angle at different frequencies, and potential and current density values of the coating under corrosive environmental conditions are measurable. The measured properties provide clues about the corrosion resistance of the coating. EIS data provides information about water absorption rather than noticeable changes on the coating surface and offers quantitative data on coating efficiency [59–61]. EIS data is obtained by measuring the impedance of the coating at different frequencies in response to the AC signal sent to the system. High impedance makes it difficult for corrosion to penetrate the coating and reach the metal surface. Low impedance increases the risk of corrosion. The frequency values of the AC signals used for measurement are important. They are generally in the frequency range of 10^{-2} to 10^6 Hz [62,63]. Signal drift or data distribution problems may occur in measurements made in low-frequency ranges [64–66]. In addition, water/moisture, oxygen or ion transfer and activation, which indicate corrosion, can be determined in measurements in low-frequency ranges, while properties such as the resistance of the solution to electric current and the double layer capacitance can be determined in measurements at high frequencies [67]. The phase angle property of the coating, measured at different frequencies, is related to corrosion. A study stated that in measurements made in the medium frequency range of 1–100 Hz, the phase angle and the coating resistance have a similar potential for decrease [64]. It is also stated that the phase angle measured at high frequencies such as 10kHz is related to the coating resistance and

https://doi.org/10.3390/coatings16080935

that as the phase angle increases, the resistance also increases, which can give an idea about the coating degradation [68]. This indicates that for high values of the phase angle, the coating increases its resistance while maintaining its barrier property, and for low values, degradation begins in the coating.

Predicting the factors affecting the corrosion performance of composite coatings is essential for ensuring the longevity of the material through necessary maintenance and repairs. Artificial intelligence (AI) methods have taken their place in the literature as an innovative tool for predicting the mechanical properties of coatings and have been actively used in recent years. In AI methods, prediction models are created by combining results obtained from various experiments on coating properties and information obtained from applied electrochemical tests and analyses. Table 1 presents a summary of studies in the literature on prediction models developed using artificial intelligence techniques related to coatings and uncoated metals.

An examination of AI studies conducted on coated and uncoated metals (Table 1) reveals that corrosion-related variables such as coating thickness, coating porosity, coating hardness, degree of corrosion, corrosion current density, corrosion rate, impedance, corroded surface and wear rate have been predicted. Data for these studies were generally obtained using experimental methods such as electrochemical impedance spectroscopy (EIS) analysis and polarisation testing. In studies requiring image processing, such as those involving the corroded surface, deep learning techniques were applied, whilst the artificial neural networks (ANN) method was frequently used in other studies. In applications using meta-heuristic-based algorithms, ANN models have emerged as the leading approach by a narrow margin [72]. Furthermore, in recent years, machine learning techniques have been tested, yielding high R^2 scores of over 90% [74–76]. Machine learning (ML) techniques have demonstrated the best performance, outperforming the ANN model in some studies [77]. Recent research confirms that both ANN and ML techniques were effective for predicting properties related to the corrosion of coated and uncoated metals. There are very few AI-based studies in the literature that evaluate both coated and uncoated steel together, which is the subject of this study. Within the scope of this study, the short-term and long-term frequency-dependent electrochemical impedance (Bode) response of coated (with Ni-Al) and uncoated steel following exposure to a corrosive environment was investigated. A similar study in the literature involves the prediction of the imaginary impedance value using ANN models based on EIS test results applied to uncoated Q235A steel [70]. In that study, ANN models were used to predict the imaginary impedance of three test specimens exposed to a NaCl solution, yielding R^2 scores of 0.9946, 0.9977 and 0.9993. Impedance is a variable comprising real and imaginary components. In addition to the study cited in the literature, this study tested the predictive performance of the ML technique and predicted the impedance magnitude and phase angle values, including the real part of the impedance. In this way, the parameters necessary for understanding the material's electrochemical (Bode) response were estimated.

Figure 1 provides a visual summary of some tests and parameters used to evaluate the electrochemical response of coatings applied to steel, and the machine learning model developed based on the EIS test results applied to Ni-Al-coated A36 steel used in this study.

Table 1. A summary of AI applications for predicting corrosion-related properties in coatings and uncoated metals.

Material	AI Method	Input Parameter	Predicted Feature	Purpose	Result	Ref.
Zr-based nano-ceramic coating on galvanised steel	Artificial neural network (ANN) - Adaptive neuro-fuzzy inference system (ANFIS)	- Zr concentration Temperature Solution immersion time - Solution pH	Corrosion rate	Corrosion rate estimation of galvanised steel with zirconium (Zr) based coating through polarisation test measurements.	The corrosion rate of the coating was estimated with R^2 scores of 0.9812 using the ANN model and 0.9819 using the ANFIS model.	[69]
Uncoated Q235A steel	- Artificial neural network (ANN)	- Real impedance - Corrosion time - Stray current density - Ion concentration	Imaginary impedance	Nyquist graph estimation from EIS analysis of uncoated Q235A steel.	The ANN model developed for estimating imaginary impedance yielded the highest R^2 score of 0.9993 among the three samples.	[70]
Uncoated 316L steel	- Artificial neural network (ANN)	- Image features descriptors - Immersion time - Electrode potential	Corrosion degree	Estimation of the corrosion degree of 316L steel exposed to a corrosive environment.	A correlation coefficient (R) of 0.9990 was obtained with the ANN model developed for corrosion degree estimation.	[71]
Ni–Zn electrophosphate coating on galvanised steel	- Genetic algorithm - Particle swarm optimisation - Genetic expression programming - Artificial neural network (ANN)	- Temperature - Solution pH - Current density - Nickel ion concentration	Corrosion current density (Icorr)	Predicting the corrosion behaviour of galvanised steel coated with nickel-zinc electro phosphate coating.	In estimating the corrosion current density of galvanised steel, R^2 values of 0.9999 were obtained with the ANN model and R^2 values of 0.9981 with the GEP model.	[72]
Paint-coated SS400 steel	- Generative Adversarial Network - Conditional GAN - Information maximising GAN - UNet + Vit	- Corroded surface data of steel plates	Corroded surface	Estimation of corroded surface of painted-coated steel with defects.	The lowest *RMSE* in predicting the corroded surface of painted-coat steel was obtained with UNet + ViT (0.48).	[73]

Table 1. *Cont.*

Material	AI Method	Input Parameter	Predicted Feature	Purpose	Result	Ref.
Ceramic-coated steels	- Elastic Net Regressor - Robust Regressor - Extreme Gradient Boosting Regressor - Bagging Regressor	- Hardness - Coating thickness - Applied load - Sliding velocity - Sliding distance	Wear rate	Predicting the wear rate of steel coated with different ceramic materials using machine learning techniques.	The highest R^2 score in predicting the wear rate of ceramic-coated steel was obtained with the bagging regressor model (0.93 R^2).	[74]
Zinc-coated low-carbon steel	- Extreme gradient boosting (XGBoost) - Multivariate regression - Linear regression - Random forest	- Anode material - Electroplating time - Concentrations of Purifier, Base 250 and Brightener additives. - NaOH and ZnO concentrations	Coating thickness	Estimation of coating thickness for zinc-coated low-carbon steel for corrosion resistance.	The highest prediction accuracy in coating thickness estimation was achieved with the XGBoost model (0.95 R^2 score).	[75]
Ceramic-coated steel	- Bagging - Boosting - Stacking - Weighted average - Voting - Hybrid	- Particle size - Input power and spray distance of plasma spraying - Powder Feed Rate - Primary and auxiliary gas flow rates	Porosity Hardness	Porosity and hardness estimation of ceramic-coated material coated by plasma spraying method.	The highest R^2 scores of 0.92 and 0.94 were obtained in predicting the porosity and hardness of the coatings using a hybrid ensemble learning model.	[76]
Thermal barrier coatings	- Backpropagation (BP) - Neural networks - Support vector machines (SVMs) - Principal component analysis (PCA)	- Terahertz time-domain data	Porosity	Porosity estimation of materials using thermal barrier coating.	In predicting the porosity of the coating, an R^2 value of 0.9186 was obtained using the PCA-SVM model with a dimensionality reduction technique.	[77]

Table 1. *Cont.*

Material	AI Method	Input Parameter	Predicted Feature	Purpose	Result	Ref.
Uncoated carbon steel	- Artificial neural network (ANN)	- The average temperature - The average relative humidity - Total rainfall - Time of wetness - Hours of sunshine - Cl^- and SO_2 deposition rates	Corrosion rate	Corrosion rate estimation of uncoated carbon steel using experimental data.	In predicting the atmospheric corrosion rate of carbon steel, an R^2 score of 0.9999 was obtained on the test set using the ANN model.	[78]

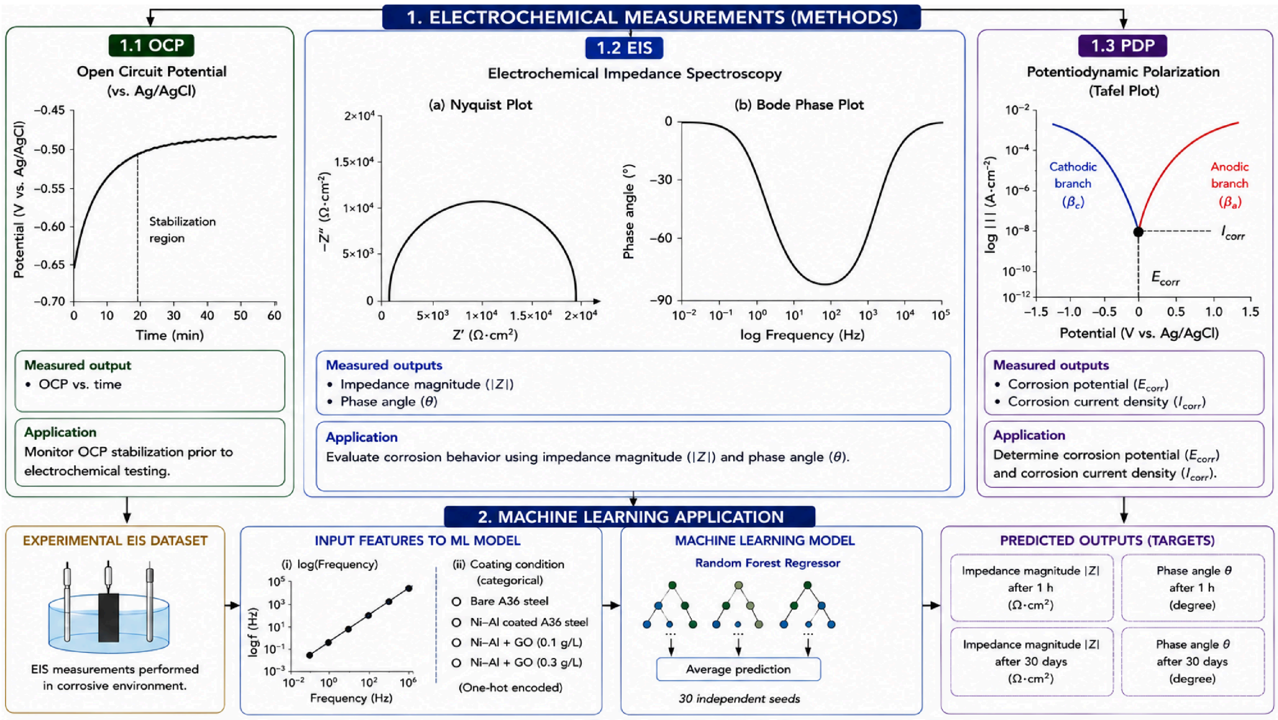

Figure 1. Electrochemical corrosion evaluation and machine learning workflow.

3. Materials and Methods

3.1. Dataset

Steel is one of the most frequently used products in structural system designs in the construction industry. Due to its structure, steel contains iron and is susceptible to corrosion due to the reaction of iron to environmental conditions. Materials exposed to water, moisture, or Cl^- ions in a corrosive environment undergo corrosion, resulting in surface deterioration and loss of various mechanical properties. To prevent this, steel and similar structural materials are coated with various elements, alloys, paints, polymers, and epoxy materials to create a barrier between the surface and the corrosive environment. The corrosion performance of coatings varies, and the wear process changes depending on the duration of exposure to the corrosive environment. This study aimed to predict the short-term and long-term frequency-dependent electrochemical impedance (Bode) response of coated and uncoated steel after exposure to a corrosive environment for 1 h and 30 days. For this purpose, the experimental results of Mehr et al. [56,79], which coated A36 steel using the plasma spraying method and exposed it to a 3.5% NaCl solution, were compiled and utilised as the dataset. The experimental results used in the study were obtained by coating A36 steel with pure nickel-aluminium (Ni-Al) powders enriched with graphene oxide dispersion in water using the plasma spray method. The dataset used was taken from the electrochemical impedance spectroscopy (EIS) experiments conducted by Mehr et al. [56,79]. The data includes EIS test results on the Bode response of (i.) uncoated A36 steel, (ii.) steel coated with Ni-Al powder, (iii.) Ni-Al-powder-coated steel treated with 100 mL of graphene oxide (GO) dispersion, and (iv.) Ni-Al-coated steel treated with 300 mL of GO after exposure to a 3.5% NaCl solution, for 1 h and 30 days.

3.1.1. Data Preprocessing

One of the most important steps in the evaluation of artificial intelligence models is the preprocessing of the data. Data preprocessing involves operations such as processing missing rows in the data, removing duplicate records, performing logarithmic transformations to numerical variables when necessary, and data categorisation. This study includes an experimental dataset containing four different cases. Firstly, empty rows in the dataset were removed. The dataset contains four categories: uncoated steel, steel coated with pure Ni-Al powder, and steel treated with 100 mL and 300 mL graphene oxide dispersion. In electrochemical impedance spectroscopy (EIS) tests in which the samples were exposed to a 3.5% NaCl solution under four different conditions, electrical signals were applied at various frequencies, and numerical impedance values were obtained. The frequency values applied in the experiment ranged from 0.01 to 100,000 Hz. A large difference between the minimum and maximum frequency values can reduce the impact of low-frequency measurements on model performance, causing high-frequency measurements to dominate the model. Therefore, a base-10 logarithmic transformation was applied to the frequency values in the dataset to ensure a balanced effect of the frequency variable on the model. The coated status in the dataset is represented in 4 columns using the one-hot encoding method. For each sample, the column corresponding to the coating is coded as 1, while the other columns take the value 0. In the data preprocessing stage, these four coated columns were later converted into a single category.

3.1.2. Dataset Characteristics

The dataset contains a total of 311 rows. The input variables of the model were the coating status and the frequency applied for electrochemical impedance spectroscopy (EIS), while the output variables were the impedance and phase angle values obtained from the EIS test after 1 h and 30 days. Several rows of processed data are shown in Table 2. Statistical properties of the data are presented in Table 3. In Table 2, the coating status is categorised as A36, S0, S1, and S2. A36 represents uncoated steel, S0 represents steel coated with pure Ni-Al, S1 represents steel enriched with 100 mL of graphene oxide (GO) dispersion, and S2 represents steel treated with 300 mL of GO. In Table 2, log_freq indicates the frequency with a logarithmic conversion applied to base 10. The impedance values of steel exposed to NaCl solution after 1 h and 30 days are denoted by |Z|_1h and |Z|_30d, respectively, and the phase angle values are denoted by phi_1h and phi_30d, respectively.

Table 2. A few rows from the dataset.

Category	log_freq	|Z|_1h	phi_1h	|Z|_30d	phi_30d
S0	1.1818	186.8365	17.5579	164.3169	18.7604
A36	3.6364	53.0305	1.8394	54.7026	0.6746
S2	3.9091	56.9189	7.5476	56.1968	8.2917
S1	−0.8182	1347.343	20.8467	247.4058	31.7233
S0	−1.1818	887.2332	37.5228	383.7254	17.8849
A36	0.2728	121.1933	27.9328	87.2334	17.4005
S1	4.8182	56.8905	7.0764	52.0320	4.9055
S2	3.8182	57.6524	8.2638	57.1764	9.0971
S0	4.7273	58.5641	3.7998	48.3497	4.0257
A36	2.9091	54.9840	3.9131	55.1318	1.7197

Table 3. Data statistical properties.

	log_freq	|Z|_1h	phi_1h	|Z|_30d	phi_30d
Mean	1.51	442.91	18.88	180.87	14.02
Std	2.04	549.40	11.68	170.35	8.79
Min	−2	52.30	1.46	48.31	0.66
Max	5	2132.11	44.05	867.15	37.38
25%	−0.27	62.41	8.36	57.36	6.67
50%	1.55	151.50	18.22	108.19	13.01
75%	3.27	685.85	27.14	253.52	19.63

https://doi.org/10.3390/coatings16080935

The correlation matrix showing the relationship between dependent and independent variables in the data is given in Figure 2. The graph visualising the relationship of independent variables with other variables, coloured by categories, is shown in Figure 3.

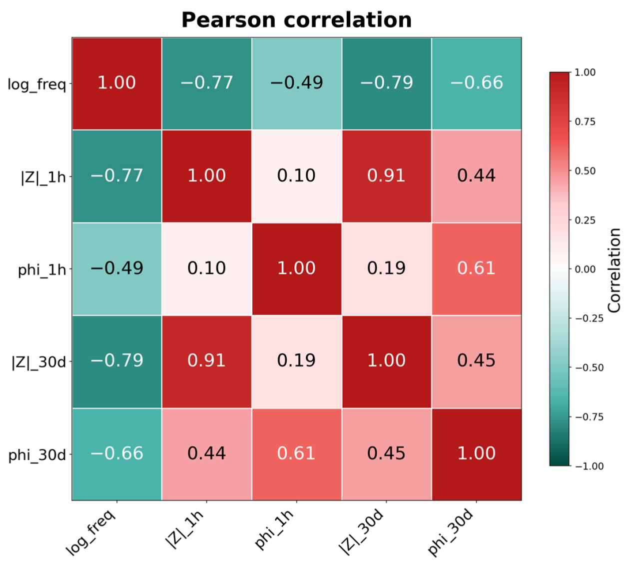

Figure 2. Correlation matrix.

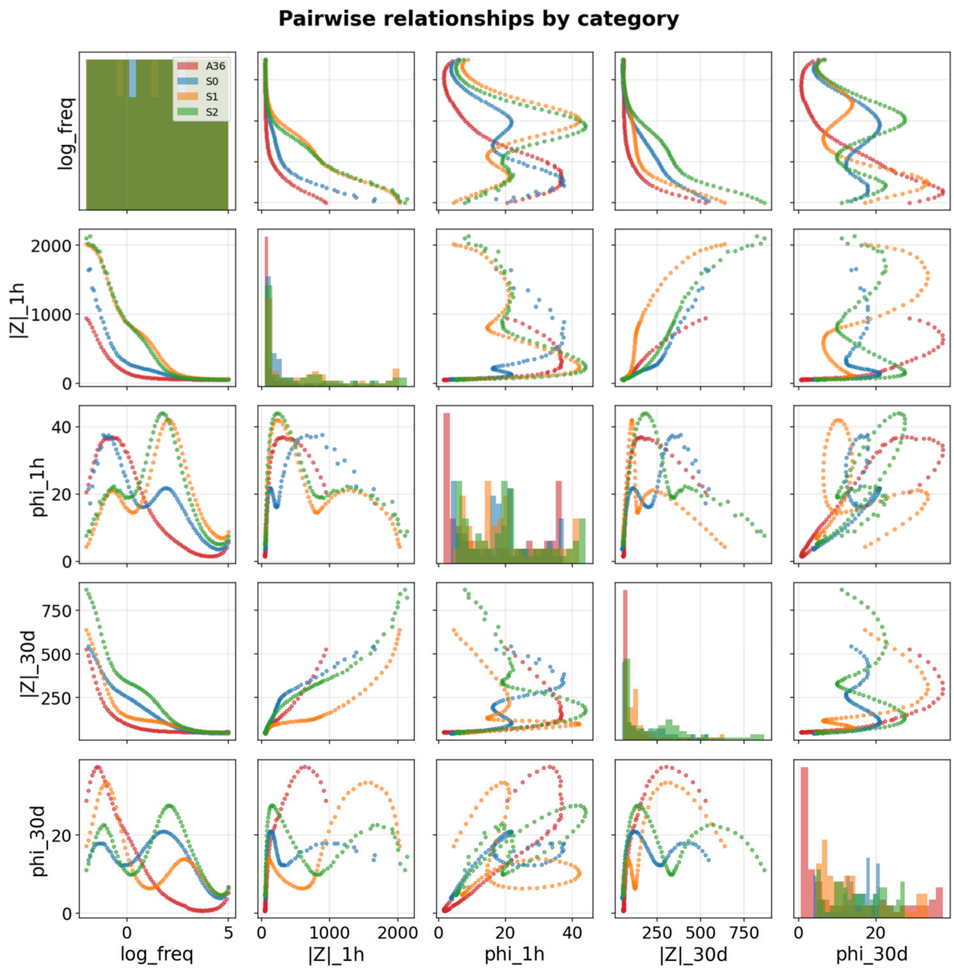

Figure 3. Pairwise relationships between numerical variables such as frequency, impedance magnitude, and phase angle for a dataset containing different coating conditions.

3.2. Machine Learning

Machine learning is an artificial intelligence method in which machines learn the relationship between independent variables (input) in a dataset and the predicted target dependent variables (output), enabling them to make inferences. The machine is first provided with a dataset for training, allowing it to learn the relationship between the input and the desired output. The machine then creates a model based on what it has learned, and the predictive accuracy of the developed learning model is tested using a set of data the machine has not previously seen. A significant part of the analysis, data interpretation and modelling stages proceed according to algorithmic approaches [80]. Machine learning models are applied to classification and regression problems. If the machine is expected to predict a group, category, or class based on the knowledge acquired through training, the problem is treated as a classification problem. If the machine is expected to predict a numerical value, the problem is treated as a regression problem. Various machine learning algorithms are used in the development of learning models. In this study, the random forest (RF) algorithm was used to predict the impedance magnitude and phase angle obtained from electrochemical impedance spectroscopy (EIS), which are used to evaluate the corrosion-related electrochemical behaviour of the coatings. The problem was formulated as a regression task, and a random forest regression model was developed.

As the study utilised a small, structured tabular dataset comprising 311 frequency-dependent Bode measurements of impedance magnitude and phase angle across four coating conditions, random forest was selected to predict the coating responses after 1 h and 30 days. Artificial neural networks have frequently been employed in previous studies; however, neural network architectures may contain a large number of trainable parameters relative to the limited number of independent experimental observations available in the present study. Under such conditions, their performance may be sensitive to network architecture, learning rate, weight initialisation, regularisation and stopping criteria, thereby increasing the risk of unstable estimates and overfitting.

Random forest was therefore adopted as a tree-based ensemble method suitable for modelling nonlinear relationships and interactions between log-frequency and coating condition without requiring a predefined functional form. Through bootstrap aggregation and random feature selection, it reduces the variance associated with individual decision trees and generally provides stable performance on small tabular datasets. Unlike K-nearest-neighbour regression, it does not rely directly on distance calculations and is therefore less sensitive to feature scaling and the choice of a distance metric. Compared with support vector regression, it avoids the need to select a kernel function, although its own hyperparameters must still be appropriately tuned. Gradient-boosting methods can also perform effectively on small datasets, but their sequential fitting procedure may make their performance more sensitive to learning rate, tree depth, regularisation and the number of boosting iterations.

These considerations support the selection of random forest as a balanced modelling approach in terms of nonlinear predictive capacity, computational efficiency, robustness and interpretability, including the possibility of conducting feature-importance and partial-dependence analyses. Nevertheless, this selection does not establish the general superiority of random forest over artificial neural networks or other machine learning methods. Rather, it indicates that, for the present limited tabular dataset, random forest provides a practical alternative to a comparatively high-parameter neural network model with lower implementation complexity and potentially lower hyperparameter sensitivity.

Random Forest Algorithm

Developed by Breiman (2001) [81], it is a tree-based machine learning (ML) algorithm. In this method, decision trees are created from randomly selected samples from the data, and model inference is made from the predictions of these trees. Decision trees have a structure consisting of nodes, with the root node at the top. Sub-nodes are formed in each node according to the selected feature. The random forest algorithm adds randomness when creating decision trees and, when splitting a node, instead of searching for the best feature from the data, it searches for the feature that provides the best split from the randomly selected features [82]. If the problem is regression, the average predictions of the trained decision trees are taken, and for classification, the final prediction is decided according to the majority class. Figure 4 shows a visual diagram summarising the flow of the random forest regressor.

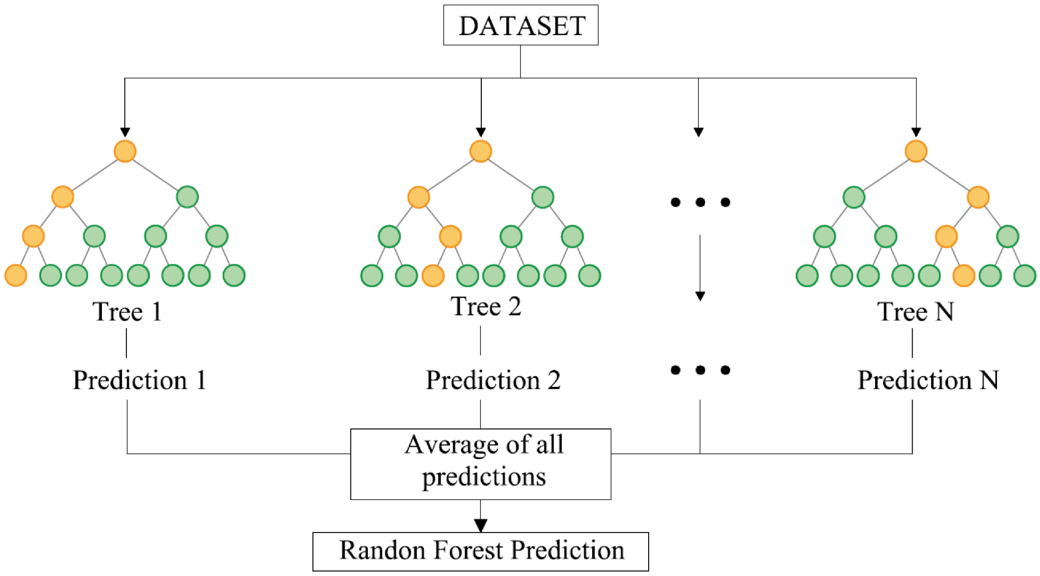

Figure 4. Representative image for random forest regressor.

3.3. Model Evaluation Metrics

Various performance metrics are used in evaluating machine learning models. These metrics vary depending on the type of problem. They provide information on how accurately the machine makes inferences for the variable predicted by the model. In this study, numerical values were predicted. For regression-type problems where numerical values are predicted, the R-squared (R^2) coefficient of determination metric is frequently used in evaluating developed models. This value represents the ability to explain variance in the data. Besides R^2, model metrics such as mean absolute error (*MAE*), mean absolute percentage error (*MAPE*), root mean squared error (*RMSE*), and mean squared error (*MSE*) are used for regression problems. Furthermore, metrics such as *Max Error*, which measures the maximum error in the model's predictions, and *Explained Var*, which measures how much of the variance in the target variable it explains, can also be used in evaluating regression models. Equation (1) shows the formula used to calculate the R^2 score [83]. The *MAE*, *MAPE*, *MSE* and *RMSE* metrics of the model are shown in Equations (2)–(5) [83], respectively. The calculation equations for *Max Error* and *Explained Variance* scores are given in Equations (6) and (7), respectively [84].

$$R^2 = 1 - \frac{\sum_{i=1}^{N}(y_i - \hat{y}_i)^2}{\sum_{i=1}^{N}(y_i - \overline{y}_i)^2} \tag{1}$$

$$MAE = \frac{1}{N}\sum_{i=1}^{N}|\hat{y}_i - y_i| \tag{2}$$

$$MAPE = 100\frac{1}{N}\sum\nolimits_{i=1}^{N}\left|\frac{y_i - \hat{y}_i}{y_i}\right| \tag{3}$$

$$MSE = \frac{1}{N}\sum_{i=1}^{N}(\hat{y}_i - y_i)^2 \tag{4}$$

$$RMSE = \sqrt{\frac{1}{N}\sum_{i=1}^{N}(\hat{y}_i - y_i)^2} \tag{5}$$

$$Max\ Error(y, \hat{y}) = \max(|y_i - \hat{y}_i|) \tag{6}$$

$$Explained\ Variance(y, \hat{y}) = 1 - \frac{Var\{y - \hat{y}\}}{Var\{y\}} \tag{7}$$

In the equations, the number of observations is denoted by N. The true value of an observation, the mean of the observed values, and the predicted values for that observation are denoted by y_i, $\overline{y}_i$, and $\hat{y}_i$, respectively. In the equations, the vector consisting of all true values is denoted by y, and the vector consisting of all predicted values is denoted by $\hat{y}$. Var is the variance of the dataset formed by the expression given in parentheses in the equation.

3.4. Model Evaluation

In machine learning models, various evaluation methods are used to test the training success of the model. One of the most common uses is to separate the dataset for training and testing, and to evaluate the model based on the machine learning from the training data and the predictions it makes using the test data it has not seen before. In a dataset that is separated to a certain extent, the data content allocated for training and testing can affect the model's performance. Due to the way the dataset is separated, the dataset is divided into training, test, and validation parts in different ways to improve the generalisation performance of the model, and thus the change in model performance for different dataset separations can be observed. The k-fold cross-validation technique, proposed by Eddy and Geisser [85,86], is a validation method based on the reuse of data. In this method, the data is divided into k parts: k-1 parts for training and 1 part for testing, creating k different folds. The final model performance is calculated by taking the average of the k-folds. Figure 5 shows a schematic representation of a 5-fold cross-validation example.

Figure 5. Five-fold cross-validation [87].

In this study, the dataset was divided into 80% training and 20% holdout data. The holdout data has never been seen by the model during the training phase. The 10-fold cross-validation technique was applied to the 80% training dataset, where the model was cross-validated 10 times, and regression metrics were calculated for both training and validation sets. Then, the model was retrained with all the training data, and the final performance values were obtained using the 20% holdout test data that the machine had not previously encountered. Since the electrochemical impedance spectroscopy (EIS) dataset consists of frequency-dependent measurements acquired from the same reference coating systems, individual observations are not statistically independent. Accordingly, the adopted random train-holdout split was intended to evaluate the model's ability to reproduce the frequency-dependent impedance response within the investigated coating systems rather than to assess generalisation to previously unseen coating formulations. Therefore, the reported predictive performance should be interpreted as interpolation across the measured impedance spectra of the investigated coatings.

The multi-seed evaluation method was employed to assess the algorithmic stability of the random forest model with respect to stochastic variations arising from random train–holdout partitioning and model initialisation. In this approach, the model was repeatedly trained using different random seeds, and the consistency of its predictive performance was evaluated by calculating the mean and standard deviation of the performance metrics across all runs. Previous studies have suggested that approximately 20 random seeds are sufficient for datasets containing around 500 samples and 10 random seeds for datasets containing approximately 1000 samples [88]. Since the present study utilised a dataset comprising 311 frequency-dependent EIS observations, a total of 30 random seeds were adopted to provide a robust assessment of algorithmic stability. For each seed, the dataset was randomly divided into 80% training and 20% holdout subsets. A 10-fold cross-validation procedure was then performed on the training subset for model development, and the optimised model was subsequently evaluated using the corresponding holdout subset. The regression performance metrics were computed for each seed, and their mean and standard deviation were used to quantify the sensitivity of the random forest model to stochastic variations in data partitioning and model training. It should be noted that this analysis evaluates the algorithmic stability of the proposed modelling framework for the investigated dataset and should not be interpreted as evidence of generalisation to previously unseen coating systems or independent experimental datasets.

4. Results and Discussion

The behaviour of A36 steel was evaluated under different coating conditions. For this purpose, data was collected from an experimental study [56] on A36 steel, A36 steel coated with pure Ni-Al powders, and A36 steel samples coated with Ni-Al enriched with 100 mL and 300 mL graphene oxide (GO) dispersion. The predictive model was developed from the dataset [79] consisting of the results obtained by exposing coated and uncoated steels to a 3.5% NaCl solution and applying electrochemical impedance spectroscopy (EIS) tests. As input to the developed predictive model, the frequency values of the electrical signal applied to the coated and uncoated steel samples in the EIS test and four different coating conditions of the steel (uncoated steel, steel coated with pure Ni-Al, steel coated with Ni-Al reinforced with 100 mL and 300 mL GO) were taken. The predicted properties are the impedance magnitude (|Z|_1h, |Z|_30d) and phase angle (phi_1h, phi_30d), which together constitute the frequency-dependent electrochemical impedance (Bode) response of A36 steel after 1 h and 30 days of exposure to a corrosive environment. The model utilised a random forest algorithm, dividing the 311-row dataset into 80% train and 20% holdout sets, and applying a 10-fold cross-validation technique. The performance consistency of the random forest model was investigated using different random seeds (30 seeds). The mean and standard deviations of the performance metrics of the random forest model using 30 seeds were calculated. Tables 4 and 5 show the performance results obtained for

https://doi.org/10.3390/coatings16080935

the impedance magnitude prediction after 1 h (|Z|_1h) and 30 days (|Z|_30d) exposure of the steel to NaCl solution, respectively. Box and whisker plots showing the metric distribution across 30 seeds for metrics |Z|_1h and |Z|_30d are given in Figures 6 and 7, respectively. The metrics based on 30 seeds (mean ± standard deviation) graphs for |Z|_1h and |Z|_30d are shown in Figures 8 and 9, respectively.

Table 4. Performance metrics for a random forest model predicting the impedance magnitude of steel exposed to a corrosive environment after 1 h.

	|Z|_1h		
	Train Mean ± Std	**CV Mean ± Std**	**Holdout Mean ± Std**
R^2	0.9995 ± 0.0001	0.9956 ± 0.0006	0.9974 ± 0.0011
Explained Var	0.9995 ± 0.0001	0.9956 ± 0.0006	0.9975 ± 0.0011
MAE	5.968 ± 0.3418	17.661 ± 0.8675	14.576 ± 2.2635
MAPE	0.0134 ± 0.0008	0.0410 ± 0.0020	0.0351 ± 0.0064
MSE	154.655 ± 17.011	1308.460 ± 174.654	777.358 ± 320.768
RMSE	12.418 ± 0.6809	36.095 ± 2.4050	27.353 ± 5.4930
Max Error	96.027 ± 18.795	259.503 ± 44.988	121.520 ± 42.7012

Table 5. Performance metrics for a random forest model predicting the impedance magnitude of steel exposed to a corrosive environment after 30 days.

	|Z|_30d		
	Train Mean ± Std	**CV Mean ± Std**	**Holdout Mean ± Std**
R^2	0.9992 ± 0.0002	0.9924 ± 0.0020	0.9952 ± 0.0016
Explained Var	0.9992 ± 0.0002	0.9925 ± 0.0020	0.9953 ± 0.0016
MAE	2.3305 ± 0.0951	7.1350 ± 0.4618	6.1219 ± 1.1630
MAPE	0.0100 ± 0.0003	0.0308 ± 0.0016	0.0264 ± 0.0033
MSE	22.598 ± 3.775	215.144 ± 48.731	145.671 ± 59.964
RMSE	4.740 ± 0.369	14.585 ± 1.580	11.827 ± 2.446
Max Error	27.017 ± 5.827	81.980 ± 19.264	49.333 ± 12.571

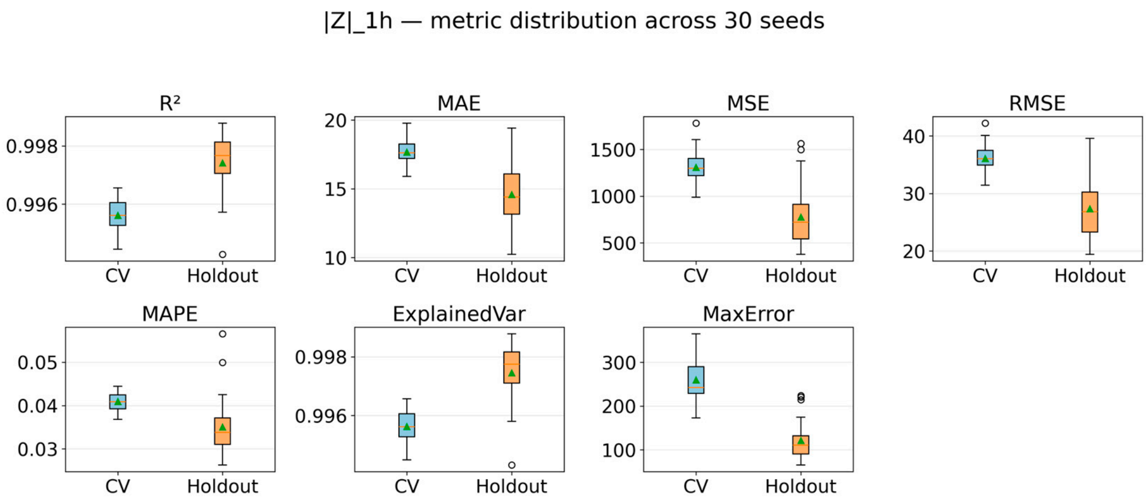

Figure 6. Box and whisker plots summarising performance metric distribution across 30 seeds for the model's |Z|_1h output.

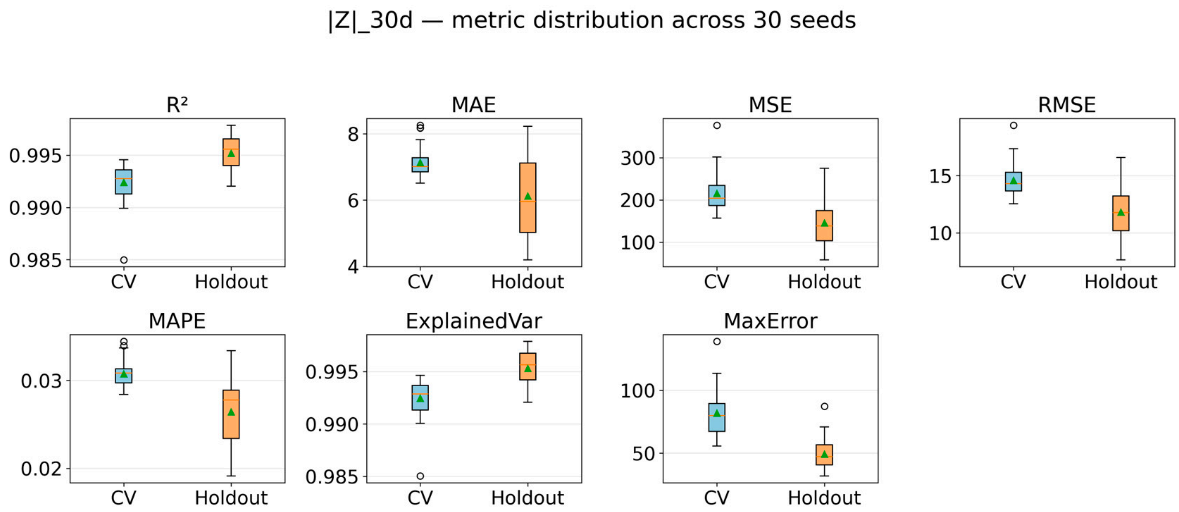

Figure 7. Box and whisker plots summarising performance metric distribution across 30 seeds for the model's |Z|_30d output.

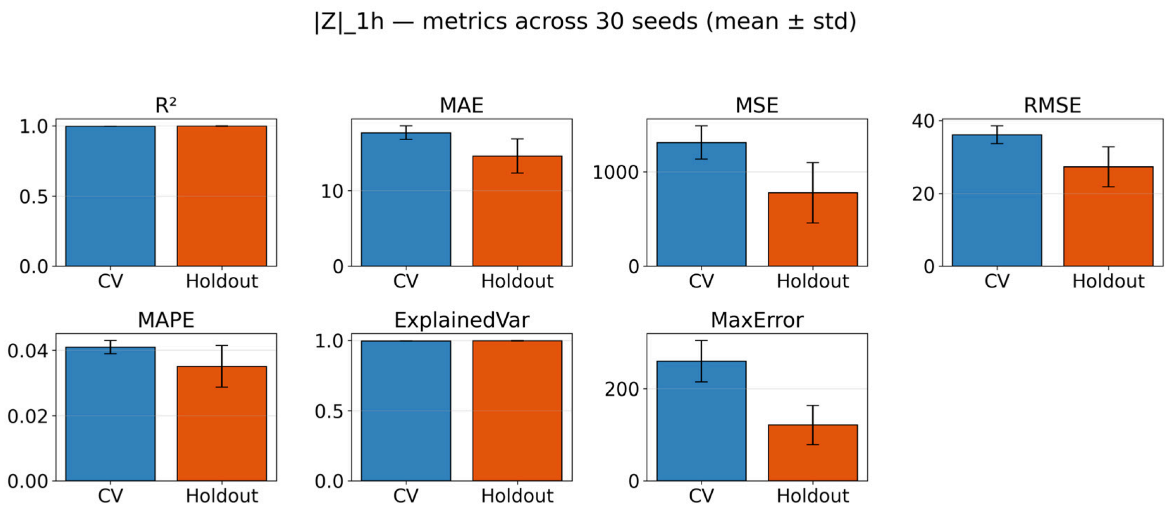

Figure 8. Bar graph of measurements obtained from 30 seeds for output |Z|_1h (mean ± standard deviation).

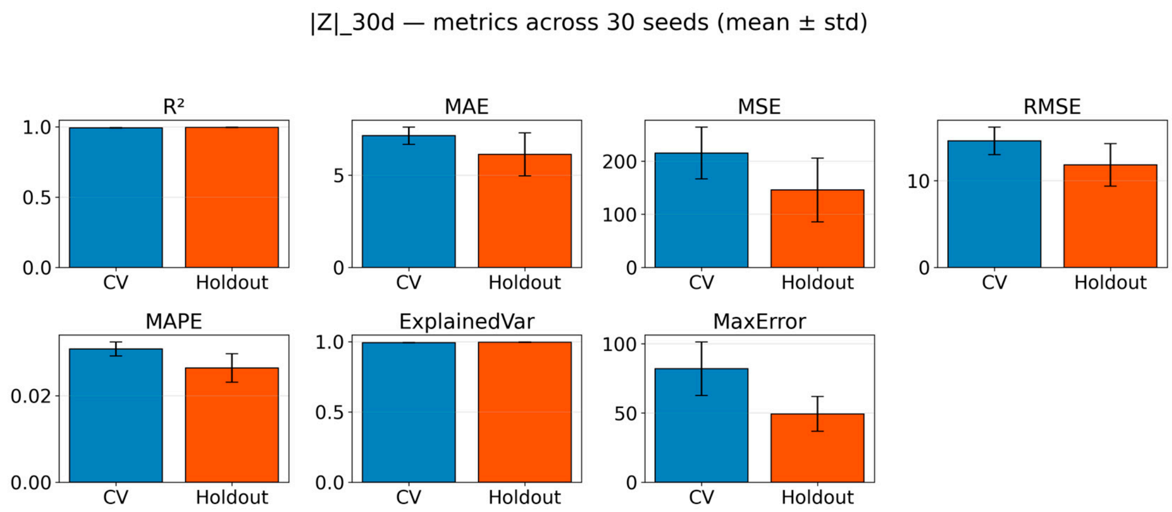

Figure 9. Bar graph of measurements obtained from 30 seeds for output |Z|_30d (mean ± standard deviation).

When examining the random forest metrics developed for predicting the impedance magnitude (|Z|_1h and |Z|_30d) of steel after 1 h and 30 days (Tables 3 and 4 and Figures 8 and 9), it is observed that the R^2 score of the random forest models exceeds 99% for the train, cv (validation), and holdout sets. This demonstrates that the model can explain the variance in the data with excellent performance. Furthermore, the low standard deviation (0.0006 for |Z|_1h and 0.002 for |Z|_30d in the validation metric) shows that the R^2 scores of the 10 folds have an insignificant difference, ranging from 0.9950 to 0.9962 for |Z|_1h and 0.9904 to 0.9944 for |Z|_30d. This indicates that the model has a stable structure on the dataset used. When examining the R^2 score and train score obtained with the holdout set, which the model had never seen before, it is understood that the difference between the train and holdout R^2 scores is less than 5% for both the |Z|_1h and |Z|_30d outputs (difference = 0.21% and difference = 0.40%). The model can accurately predict the electrochemical response of steel exposed to a corrosive environment without overfitting. The explained variance scores obtained for both outputs are almost identical to R^2. The similarity of the explained variance scores to R^2 indicates that the model's error distribution is balanced. The tables show that the |Z|_1h output has an error margin of 15 units in the holdout set and the |Z|_30d output has an error margin of 6 units (*MAE*). When examining the minimum and maximum values of |Z|_1h and |Z|_30d in Table 2, the impedance magnitude (|Z|_1h) values 1 h after the event range from a minimum of 52.30 to and the maximum is 2132.11, while the impedance magnitudes 30 days later (|Z|_30d) range from a minimum of 48.31 to a maximum of 867.15 units. According to the *MAE* and *MAPE* scores, an error of 15 units for |Z|_1h indicates a deviation of approximately 3.5% from the true value, and an error of 6 units for |Z|_30d indicates a deviation of approximately 2.6% from the true value. This margin of error indicates that the model makes predictions that deviate from the true value at a tolerable level. The max error metric indicates the model's most inaccurate prediction in the sample. In the holdout set, the max error for the |Z|_1h output was approximately 121.5 units, and for the |Z|_30d output, it was approximately 49.3 units. The max error may increase as the number of outliers in the sample increases. The max errors presented in the tables and figures show, for both outputs, how much the model's most inaccurate prediction on the sample deviates from the true value. Accordingly, the max error calculated for the |Z|_1h output is higher than that for the |Z|_30d output. However, the maximum value of |Z|_1h in the data is 2132. This level of error appears to be tolerable for the high values of |Z|_1h. Additionally, the metrics presented in the tables are the means of 30 seeds for the random forest model. The reported means and standard deviations of the metrics indicate that the model is stable on the dataset used, even though the random division of the data did not yield optimal results.

The R^2 and *RMSE* metrics for the validation (cv) and holdout sets obtained from the random forest model across 30 seeds are shown in Figures 10 and 11, respectively, for |Z|_1h, and in Figures 12 and 13, respectively, for |Z|_30d.

Upon examining Figure 10, the R^2 metrics for the |Z|_1h output yield similar results ranging from 0.994 to 0.999 across 30 seeds in both the validation (CV) and holdout sets. For the |Z|_30d output shown in Figure 12, the R^2 metrics yield similar values ranging from 0.985 to 0.998 across 30 seeds. There is no significant difference in the R^2 metrics across the 30 seeds. When examining the *RMSE* metrics for |Z|_1h and |Z|_30d across 30 seeds in Figures 11 and 13, it is evident that there are fluctuations in both the CV and holdout sets, as also observed in the R^2 metrics. However, the error does not increase continuously for each seed. This indicates that the fluctuations are due to random initial values. Furthermore, in both graphs, the holdout set showed lower error metrics than the CV set. All indicators demonstrate that there is no significant systematic error in the model and that it exhibits a stable and reproducible structure on the dataset used with respect to random initialisations.

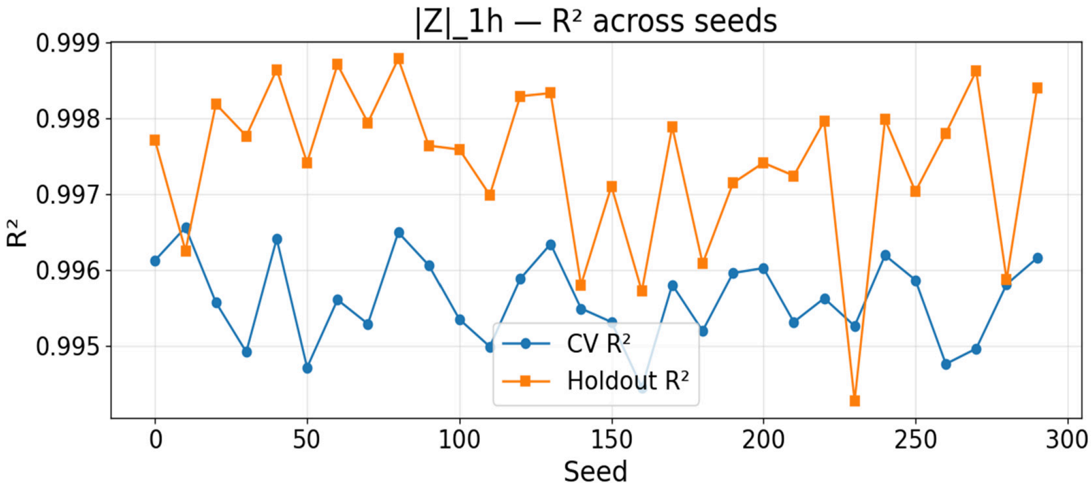

Figure 10. Graph of R^2 metrics across 30 seeds for |Z|_1h.

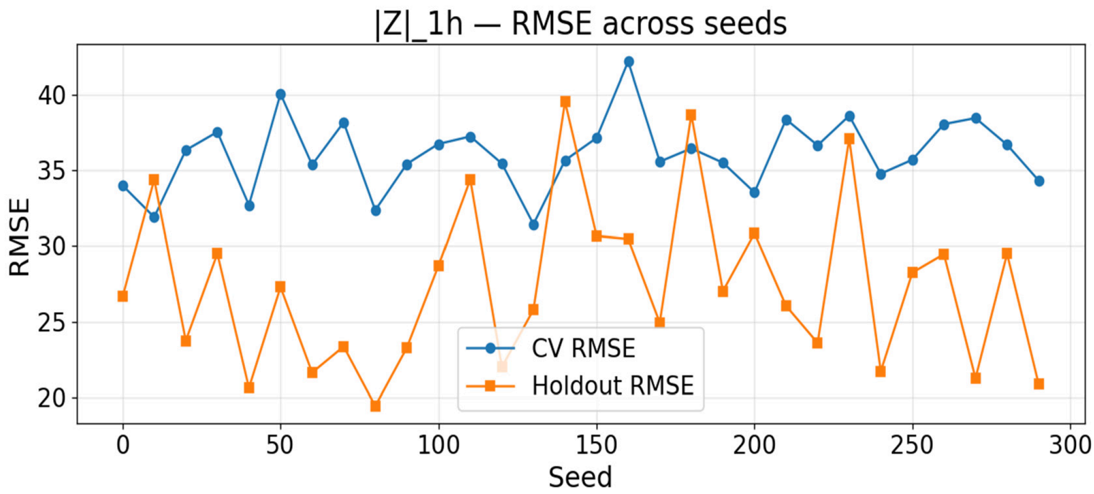

Figure 11. Graph of *RMSE* metrics across 30 seeds for |Z|_1h.

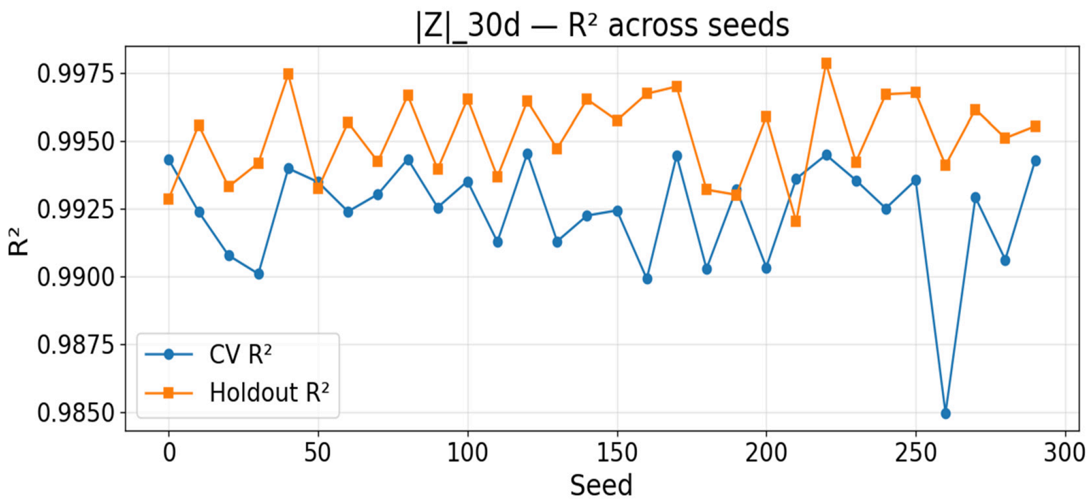

Figure 12. Graph of R^2 metrics across 30 seeds for |Z|_30d.

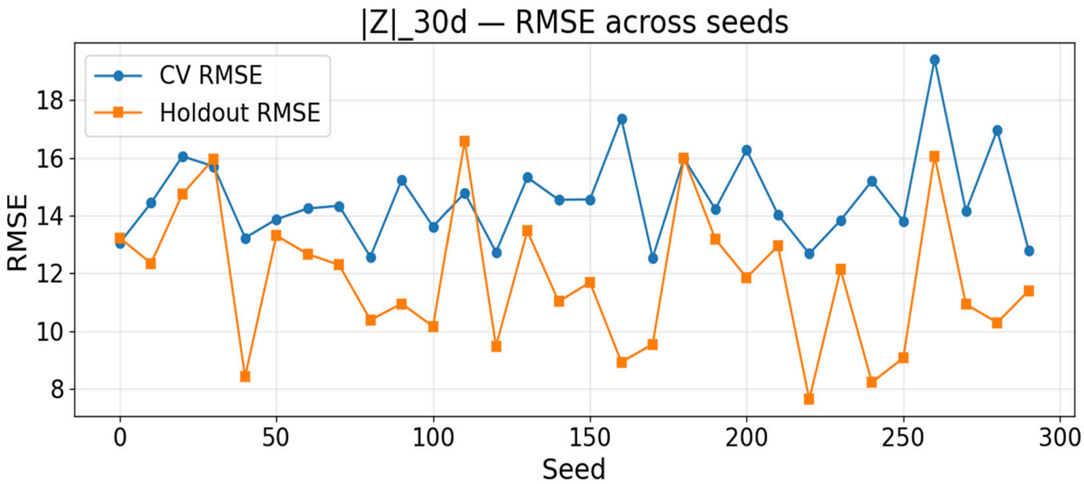

Figure 13. Graph of *RMSE* metrics across 30 seeds for ∣Z∣_30d.

In this study, a model was developed using random forest to predict the impedance magnitude and phase angle values of coated and uncoated steel exposed to a corrosive environment after 1 h and 30 days. Thirty seeds were used to analyse the stability of the model. The phase angle value of the steel after 1 h is expressed as phi_1h, and the phase angle value after 30 days is expressed as phi_30d. Tables 6 and 7 show the mean and standard deviations of the model metrics for phi_1h and phi_30d outputs at 30 seeds, respectively. Box and whisker plots showing the metric distribution for phi_1h and phi_30d outputs across the 30 seeds are given in Figures 14 and 15, respectively. Graphs of the metrics (mean ± standard deviation) based on the 30 seeds for phi_1h and phi_30d are shown in Figures 16 and 17, respectively.

Table 6. Performance metrics for a random forest model predicting the phase angle value of steel exposed to a corrosive environment after 1 h.

		phi_1h	
	Train Mean ± Std	**CV Mean ± Std**	**Holdout Mean ± Std**
R^2	0.9985 ± 0.0002	0.9863 ± 0.0019	0.9896 ± 0.0037
Explained Var	0.9990 ± 0.0001	0.9864 ± 0.0019	0.9900 ± 0.0035
MAE	0.1900 ± 0.0090	0.9370 ± 0.0447	0.8172 ± 0.1330
MAPE	0.0216 ± 0.0011	0.0676 ± 0.0043	0.0589 ± 0.0132
MSE	0.201 ± 0.023	1.848 ± 0.266	1.425 ± 0.486
RMSE	0.448 ± 0.026	1.356 ± 0.098	1.176 ± 0.206
Max Error	1.988 ± 0.393	5.693 ± 1.249	4.097 ± 1.214

Table 7. Performance metrics for a random forest model predicting the phase angle value of steel exposed to a corrosive environment after 30 days.

		phi_30d	
	Train Mean ± Std	**CV Mean ± Std**	**Holdout Mean ± Std**
R^2	0.9990 ± 0.0001	0.9905 ± 0.0018	0.9921 ± 0.0035
Explained Var	0.9990 ± 0.0001	0.9905 ± 0.0018	0.9923 ± 0.0034
MAE	0.1900 ± 0.0090	0.5810 ± 0.0380	0.5160 ± 0.0670
MAPE	0.0203 ± 0.0023	0.0656 ± 0.0096	0.0604 ± 0.0274
MSE	0.078 ± 0.011	0.731 ± 0.142	0.589 ± 0.246
RMSE	0.278 ± 0.019	0.851 ± 0.082	0.754 ± 0.146
Max Error	1.509 ± 0.406	4.615 ± 1.365	2.856 ± 1.050

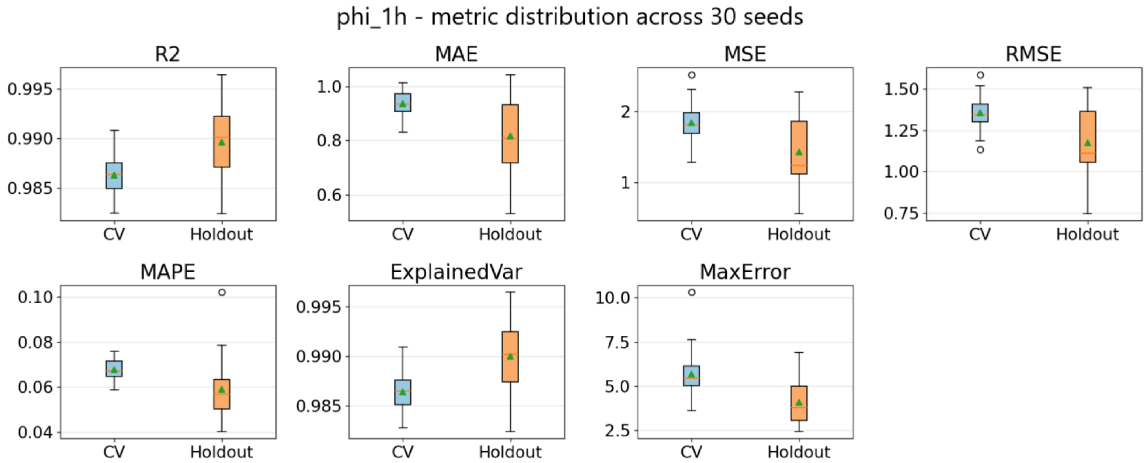

Figure 14. Box and whisker plots summarising performance metric distribution across 30 seeds for the model's phi_1h output.

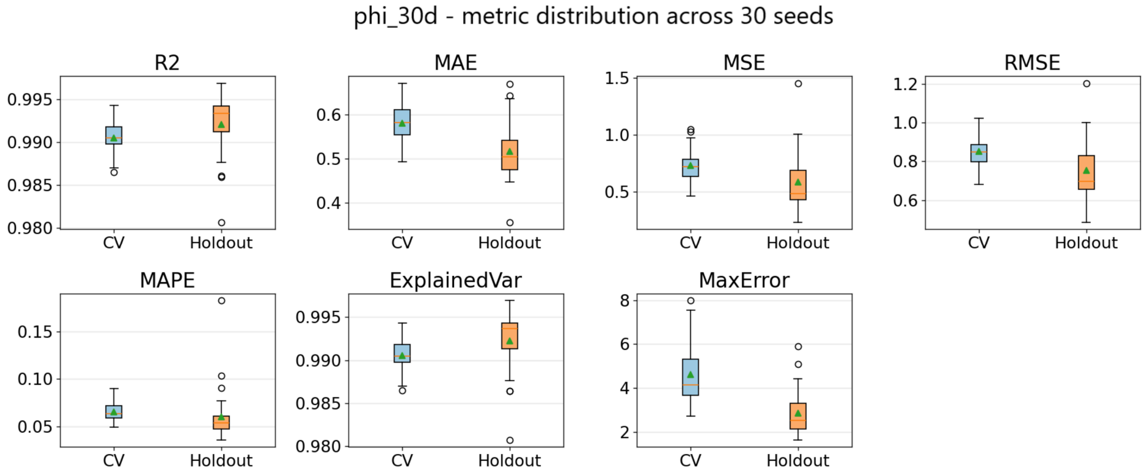

Figure 15. Box and whisker plots summarising performance metric distribution across 30 seeds for the model's phi_30d output.

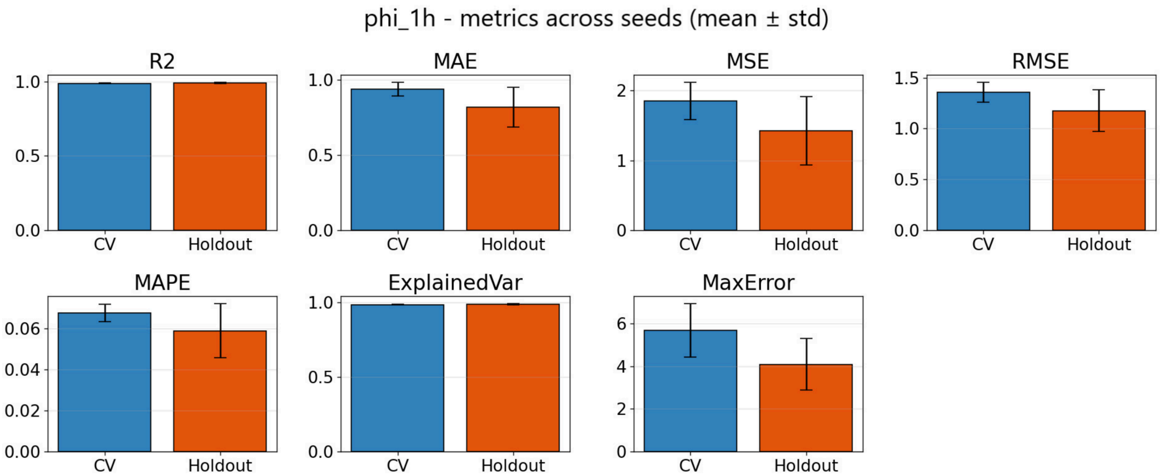

Figure 16. Bar graph of measurements obtained from 30 seeds for output phi_1h (mean ± standard deviation).

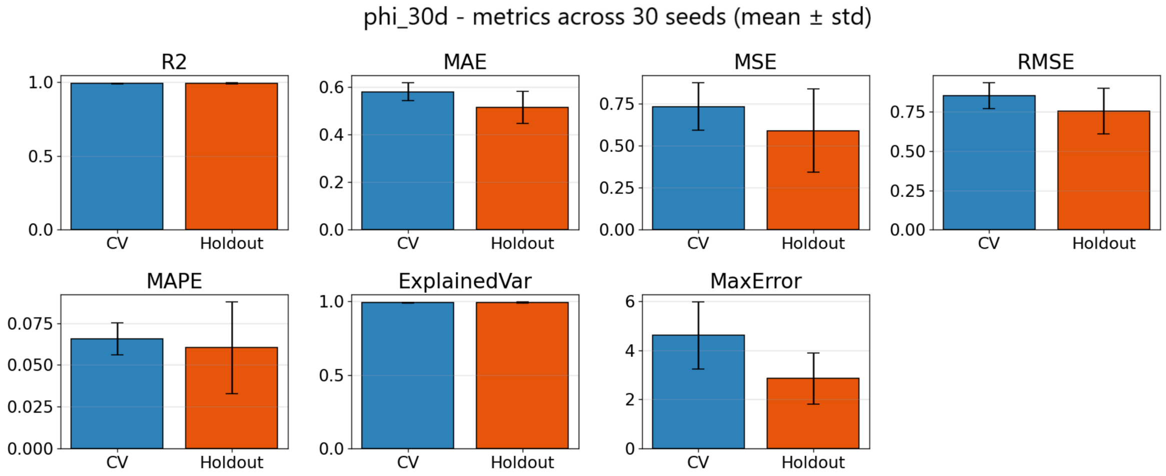

Figure 17. Bar graph of measurements obtained from 30 seeds for output phi_30d (mean ± standard deviation).

The model metrics for predicting the phase angles (phi_1h and phi_30d) of the electrochemical response of steel exposed to a corrosive environment after 1 h and 30 days are presented in Tables 5 and 6. The values in the tables represent the mean and standard deviation of 30 seeds. An examination of the R^2 scores in the tables reveals that the train, validation (CV), and holdout sets achieve approximately 99% R^2. For the phase angle (phi_1h) output after 1 h of exposure to a corrosive environment, the R^2 score for the holdout set ranges from 0.9859 to 0.9933 based on the standard deviation. For the phase angle (phi_30d) output following 30 days of exposure to a corrosive environment, the R^2 score ranges from 0.9886 to 0.9956 relative to the standard deviation. For both outputs, the model demonstrated that it could explain approximately 99% of the variation in the target variable in the data. The standard deviation resulted in low variability in performance. For the phi_1h and phi_30d outputs, the difference in mean R^2 between the train and holdout sets is approximately 0.9% and 0.7%, respectively. The fact that the difference between the train and holdout sets remains below 5% indicates that the random forest model is not overfitted. Furthermore, the fact that the explained variance values for both outputs are similar to the R^2 scores indicates that the model's error distribution is balanced. Considering the metrics and tables presented in Figures 14–17, it is evident that the random forest model makes successful predictions. The *MAE* and *MAPE* values in Tables 5 and 6 are quite low. For the Phi_1h and Phi_30d outputs, the model predicts with error margins of approximately 0.8 units and 0.5 units, respectively, on the holdout set. According to the statistical properties of the data in Table 2, the minimum and maximum values of phi_1h are 1.46 and 44.05, respectively, while those of phi_30d are 0.66 and 37.38. The reported errors are within tolerable levels. Based on the *MAPE* percentages, phi_1h deviated from the true value by approximately 5.9% and phi_30d by 6% in the holdout set. Looking at the maximum error values, the worst prediction deviation is 4.1 degrees for phi_1h and 2.9 degrees for phi_30d. In electrochemical impedance spectroscopy (EIS) testing, differences in phase angle may be observed depending on frequency values and measurement conditions. In this case, the maximum error values can be considered a tolerable level of measurement error.

The R^2 and *RMSE* metrics for the validation (cv) and holdout sets obtained from the random forest model across 30 seeds are shown in Figures 18 and 19, respectively, for phi_1h, and in Figures 20 and 21, respectively, for phi_30d.

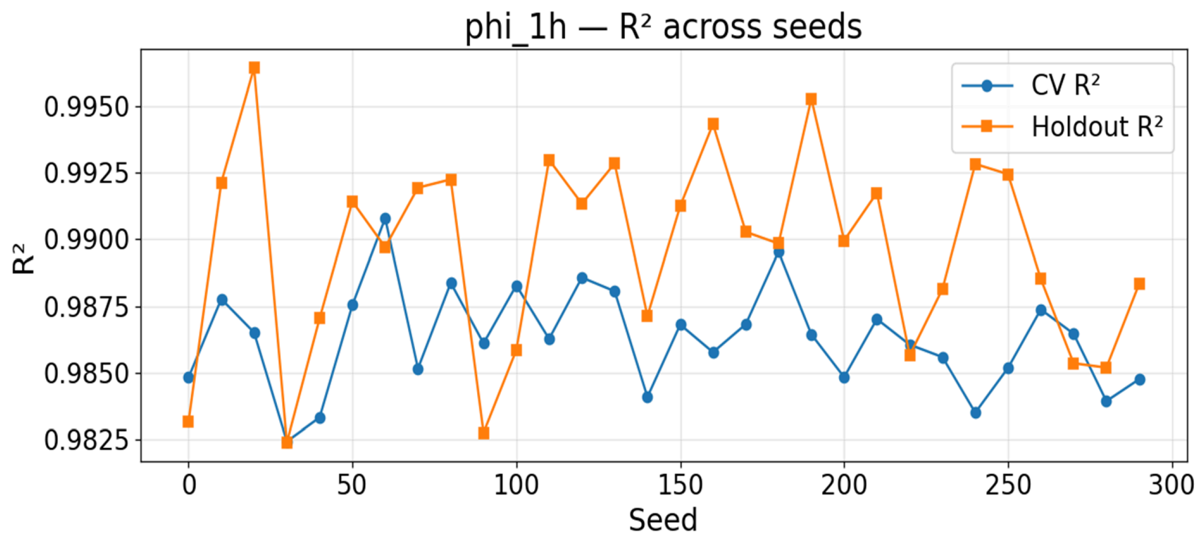

Figure 18. Graph of R^2 metrics across 30 seeds for phi_1h.

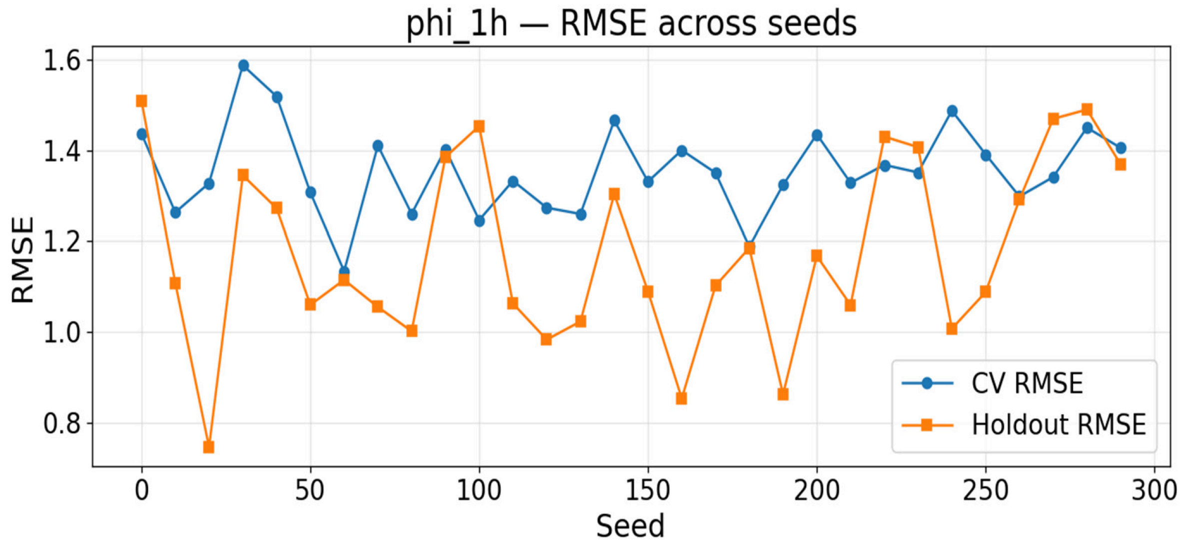

Figure 19. Graph of *RMSE* metrics across 30 seeds for phi_1h.

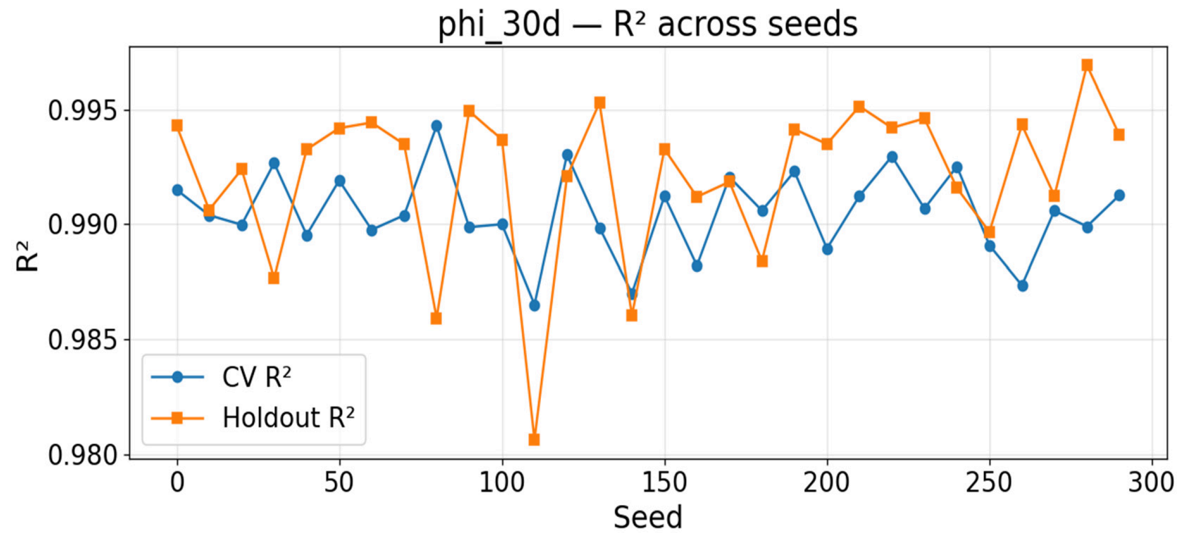

Figure 20. Graph of R^2 metrics across 30 seeds for phi_30d.

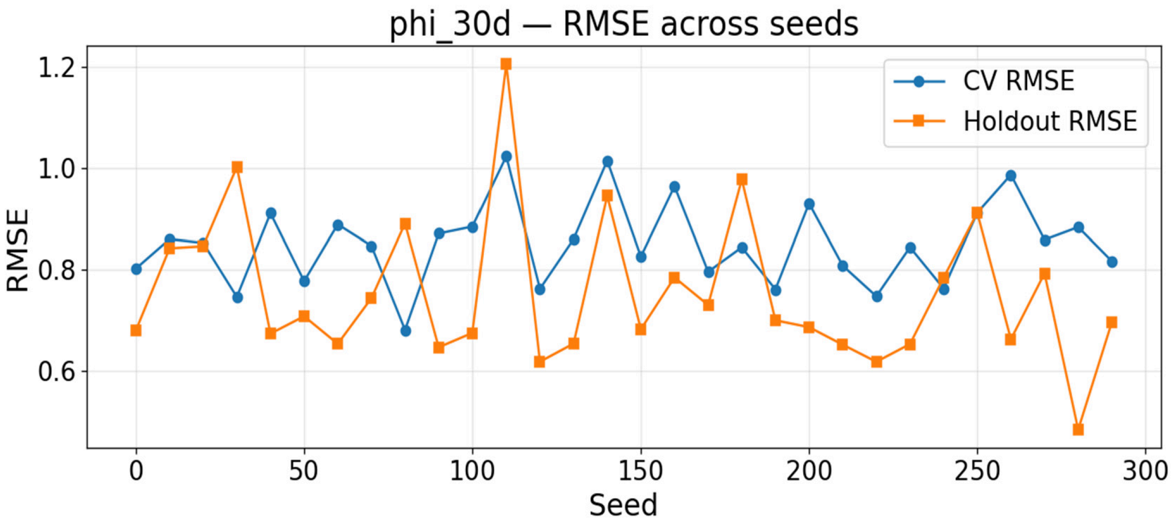

Figure 21. Graph of *RMSE* metrics across 30 seeds for phi_30d.

An examination of Figure 18 reveals that the R^2 metrics for the phi_1h output yield similar results in the validation (CV) and holdout sets, ranging between 0.983 and 0.996 across 30 seeds. For the phi_30d output shown in Figure 20, the R^2 metrics show values ranging from 0.980 to 0.996 across 30 seeds. In the holdout set, the maximum performance difference across all seeds was 1.3% for the phi_1h output, whilst it was 1.6% for the phi_30d output. There was no significant difference across the 30 seeds. Furthermore, the model's R^2 scores on the holdout set generally exceeded the CV metrics for both outputs. Although fluctuations were observed in the performance metrics graph for the 30 seeds, the R^2 scores did not show a consistent trend of increasing or decreasing as the seed changed. The difference is due to variations in the model's performance arising from different initial values of data. Despite the fluctuations in the graph, the maximum and minimum differences in R^2 performance across the two outputs, 1.3% and 1.6% respectively, represent an acceptable margin of variation. The model has demonstrated consistent results and stability on the dataset used across all seed values. When examining the *RMSE* metrics for 30 seeds for phi_1h and phi_30d in Figures 19 and 21, it is evident that there are fluctuations in both the CV and holdout sets. As seen in the R^2 plot, the error did not consistently increase or decrease across all seeds. This is an indication that it stems from random initial values. Furthermore, according to the *RMSE* metrics, for most seeds, the holdout set yielded lower error metrics than the CV in both plots. All indicators show that the model can produce predictions with a tolerable level of error and, thanks to its stable structure on the dataset used, is reproducible.

In the literature, studies on the prediction of the electrochemical (Bode) response of coated and uncoated metals are quite limited. Artificial neural network (ANN) models are frequently used in generalised models for predicting the corrosion-inhibiting properties of coatings, and machine learning methods have been the subject of research in recent years. In one source relevant to the subject of this study, the EIS analysis of uncoated Q235A steel was evaluated, and the imaginary impedance values of three different uncoated specimens exposed to a NaCl solution were predicted using an ANN model [70]. The focus of this study was to predict the impedance magnitude and phase angle values taking into account the imaginary and real components of impedance for uncoated A36 steel and A36 steel coated with Ni-Al in three different ways. The study is innovative in that it utilises a random forest (i.e., machine learning technique), employs the multi-seed method to assess model stability, and provides insights into the material's electrochemical response by predicting the Bode response (impedance magnitude and phase angle) for both coated and uncoated steel.

5. Conclusions

As part of this study, a random forest model was developed to predict the short- and long-term frequency-dependent electrochemical impedance (Bode) response of coated and uncoated steel when exposed to a corrosive environment. To this end, experimental results of uncoated A36 steel and steel with nickel–aluminium (Ni-Al) coating, obtained from electrochemical impedance spectroscopy (EIS) tests [56,79], were compiled to form a dataset. Four different coating options were considered: uncoated A36 steel, steel coated with pure Ni-Al powder, and Ni–Al-coated steels enhanced with 100 mL and 300 mL graphene oxide (GO) dispersions. The frequency of the electrical signal applied to uncoated and coated steel exposed to a 3.5% NaCl solution, as well as the coating condition, were used as input in the development of a model to predict the material's short- and long-term electrochemical response. The short-term (1 h later) and long-term (30 days later) impedance magnitude and phase angle values of the material following exposure to the NaCl solution were predicted using a random forest model. To analyse the model's robustness against randomness, model performance was evaluated for different initial clusters using 30 seeds, and the model was validated using the 5-fold cross-validation technique.

Impedance magnitude and phase angle values reflect the material's electrochemical response and provide information about the coating's protective capability and corrosion behaviour. A high impedance value makes it difficult for factors that could cause corrosion, such as water/moisture or Cl^- ions, to reach the metal substrate through the coating. Consequently, high impedance values are generally associated with high corrosion resistance, whereas lower impedance values generally indicate easier penetration of aggressive ions through the coating, thereby promoting corrosion. The phase angle is another important indicator of the coating's electrochemical condition. As the coating deteriorates, the phase angle also changes. The effect of the phase angle varies depending on the frequency at which it is measured. As the phase angle values measured at high frequencies (such as 10 kHz) increase, the coating's barrier properties are maintained, resulting in better resistance to degradation. Low phase angle values, on the other hand, indicate that degradation of the coating has begun. It has been noted that the trend of decreasing coating resistance observed for phase angle values measured at medium frequencies (such as 1–100 Hz) is similar [64]. In determining the protective properties of the coating against corrosion in relation to the phase angle, the accurate estimation of the phase angle values measured across each frequency range is of importance. Consequently, impedance and phase angle parameters provide an indication of the coating's corrosion behaviour. The following findings were obtained in the prediction of the short- and long-term electrochemical response of coated and uncoated steel:

1. In the random forest model developed for the impedance magnitudes (|Z|_1h and |Z|_30d) and phase angles (phi_1h and phi_30d) of coated and uncoated steel following exposure to a corrosive environment for 1 h and 30 days, the R^2 scores reached 99% across all the training, cv (validation) and holdout sets, R^2 scores reached 99%.
2. The variance values explained in the Bode response (impedance and phase angle) prediction model for coated and uncoated steel are almost identical to the R^2 scores. This demonstrates that the random forest model is able to explain the variance of the target variable in the data with excellent performance and that the model's error distribution is balanced.
3. To assess the sensitivity of the random forest model to stochastic effects associated with random train–holdout partitioning, the entire modelling procedure was repeated

using 30 different random seeds. The standard deviation of the 30 seeds used for the model's algorithmic stability analysis did not exceed 2% on the holdout set.
4. The model achieved high accuracy on the holdout set for impedance (holdout R^2 of at least 99.6% for |Z|_1h and 99.4% for |Z|_30d) and phase angle (holdout R^2 of at least 98.6% for phi_1h and 98.9% for phi_30d), with a low margin of error (holdout *MAPE* 3.5% for |Z|_1h, 2.6% for |Z|_30d, 5.9% for phi_1h and 6% for phi_30d), providing predicts very close to the true values.
5. The resulting performance metrics exhibited low variability, indicating that the model training process was algorithmically stable for the investigated dataset.
6. Although the multi-seed analysis demonstrates low sensitivity of the learning algorithm to random initialisation, it should not be interpreted as evidence of generalisation to previously unseen coating systems or independent experimental datasets.

The study has successfully developed a predictive model from a limited amount of experimental data without the need for additional experimental procedures. The model provides good predictions for the investigated coated and uncoated A36 steel specimens. The model successfully predicted the short- and long-term EIS (Bode) response of coated and uncoated steel without overfitting, with a maximum error margin of 6%. The predicted EIS response was subsequently used to evaluate the corrosion-related electrochemical behaviour of the investigated specimens. In the model evaluation process, the impedance magnitudes (|Z|_1h and |Z|_30d) were retained in their original scale rather than being logarithmically transformed. Although logarithmic scaling is commonly adopted for visualising Bode plots and may be beneficial when modelling variables spanning several orders of magnitude, the impedance values in the present dataset cover approximately 1.6 decades. Furthermore, the objective of this study was to predict the absolute impedance magnitude, which provides direct physical interpretation of the electrochemical response. Since random forest regression is relatively insensitive to monotonic transformations of the target variable, the original impedance values were retained to preserve engineering interpretability of the predicted responses. It needs to be noted that the proposed random forest model accurately reproduces the frequency-dependent electrochemical impedance response of the investigated coating systems. These predicted impedance spectra can subsequently be used to assist the interpretation of corrosion-related electrochemical behaviour within the investigated experimental conditions. The applicability of the model to previously unseen coating formulations remains a subject for future investigation.

The present dataset contains impedance spectra measured for four reference coating conditions under two exposure durations. Consequently, although the dataset contains 311 frequency-dependent observations, the authors acknowledge that these observations originate from a limited number of coating systems. The machine learning model therefore just learns the relationship between frequency, coating condition and electrochemical response for the investigated systems. The reported validation demonstrates the model's ability to accurately reproduce the measured Bode response of these reference coatings. However, it should not be interpreted as evidence that the model can predict the entire impedance spectra of new coating formulations or different experimental conditions. Demonstrating such generalisation would require a substantially larger dataset containing additional coating systems and grouped validation strategies, such as leave-one-condition-out cross-validation. Furthermore, the degradation process of corrosion-induced coatings may not follow a strictly linear pattern. In the present study, the short- and long-term (after 1 h and 30 days) electrochemical response of a Ni–Al-coated steel was predicted using EIS test results obtained from a previous study. As the study from which the dataset was derived did not include intermediate exposure data, the medium-term performance of the coating could not be assessed in this study. However, despite this limitation, the proposed model successfully predicted the coating's impedance magnitude (R^2 for 1 h: 0.9974 ± 0.0011; for 30 days: 0.9952 ± 0.0016) and phase angle (R^2 for 1 h: 0.9896 ± 0.0037; for 30 days: 0.9921 ± 0.0035) with an accuracy of up to 99%, and has demonstrated the ability to accurately reproduce the electrochemical response during both the early and late stages of coating degradation.

Future studies should expand the dataset to include a larger variety of coating formulations and employ grouped validation approaches, such as leave-one-condition-out cross-validation, to evaluate the model's capability to generalise to previously unseen coating systems. In addition, it is considered that the inclusion of EIS data for intermediate exposure times represents an important aspect in interpreting the corrosion performance of the coating for future studies and may further enhance the generalisability of the proposed model.

Author Contributions: Conceptualization, A.O., G.B. and Ü.I.; methodology, A.O., G.B. and Ü.I.; software, A.O., G.B., S.M.N. and Ü.I.; formal analysis, A.O.; investigation, A.O.; data curation, A.O.; writing—original draft preparation, S.M.N., G.B. and A.O.; writing—reviewed and editing, G.B.; visualization, S.M.N., G.B. and A.O.; supervision, G.B. All authors have read and agreed to the published version of the manuscript.

Funding: This research received no external funding.

Institutional Review Board Statement: Not applicable.

Informed Consent Statement: Not applicable.

Data Availability Statement: The raw data supporting the conclusions of this article will be made available by the authors upon request.

Conflicts of Interest: The authors declare no conflicts of interest.

References

1. Sych, O.V.; Kruglova, A.A.; Schastlivtsev, V.M.; Tabatchikova, T.I.; Yakovleva, I.L. Effect of vanadium on the precipitation strengthening upon tempering of a high-strength pipe steel with different initial structure. *Phys. Met. Met.* **2016**, *117*, 1270–1280. [CrossRef]
2. Tęcza, G. Changes in Microstructure and Abrasion Resistance during Miller Test of Hadfield High-Manganese Cast Steel after the Formation of Vanadium Carbides in Alloy Matrix. *Materials* **2022**, *15*, 1021. [CrossRef] [PubMed]
3. Hai, N.H.; Trung, N.D.; Khanh, P.M.; Dung, N.H.; Long, B.D. Strain hardening of Hadfield high manganese steels. *Mater. Today Proc.* **2022**, *66*, 2933–2937. [CrossRef]
4. Luo, Q.; Zhu, J. Wear Property and Wear Mechanisms of High-Manganese Austenitic Hadfield Steel in Dry Reciprocal Sliding. *Lubricants* **2022**, *10*, 37. [CrossRef]
5. Takabe, H.; Ueda, M. The Formation Behavior of Corrosion Protective Films of Low Cr Bearing Steels in CO_2 Environments. In Proceedings of the CORROSION 2001, Houston, TX, USA, 11–16 March 2001; pp. 1–15.
6. Chen, C.; Lu, M.; Sun, D.; Zhang, Z.; Chang, W. Effect of Chromium on the Pitting Resistance of Oil Tube Steel in a Carbon Dioxide Corrosion System. *Corrosion* **2005**, *61*, 594–601. [CrossRef]
7. Sun, J.; Liu, W.; Chang, W.; Zhang, Z.; Li, Z.; Yu, T.; Lu, M. Characteristics and formation mechanism of corrosion scales on low-chromium X65 steels in CO_2 environment. *Acta Metall. Sin.* **2009**, *45*, 84–90.
8. Guo, S.; Xu, L.; Zhang, L.; Chang, W.; Lu, M. Corrosion of alloy steels containing 2% chromium in CO_2 environments. *Corros. Sci.* **2012**, *63*, 246–258. [CrossRef]
9. Sun, J.; Sun, C.; Lin, X.; Cheng, X.; Liu, H. Effect of Chromium on Corrosion Behavior of P110 Steels in CO_2-H_2S Environment with High Pressure and High Temperature. *Materials* **2016**, *9*, 200. [CrossRef] [PubMed]
10. Abdeen, D.H.; El Hachach, M.; Koc, M.; Atieh, M.A. A Review on the Corrosion Behaviour of Nanocoatings on Metallic Substrates. *Materials* **2019**, *12*, 210. [CrossRef] [PubMed]
11. Dariva, C.G.; Galio, A.F. Corrosion Inhibitors Principles, Mechanisms and Applications. In *Developments in Corrosion Protection*; Aliofkhazraei, M., Ed.; IntechOpen: Rijeka, Croatia, 2014; p. 365379.
12. Yao, M.; He, Y.; Zhang, Y.; Yang, Q. Al_2O_3-Y_2O_3 Nano-and Micro-Composite Coatings on Fe-9Cr-Mo Alloy. *J. Rare Earths* **2006**, *24*, 587–590. [CrossRef]

13. Roos, O. Brugal® thin organic coatings: Effective and gainful alternative to traditional methods of protection of steels from corrosion. *Met. Sci. Heat Treat.* **2011**, *53*, 350–352. [CrossRef]
14. Figueira, R.B. Hybrid Sol–gel Coatings for Corrosion Mitigation: A Critical Review. *Polymers* **2020**, *12*, 689. [CrossRef] [PubMed]
15. Xie, J.; Lu, Z.; Zhou, K.; Li, C.; Ma, J.; Wang, B.; Xu, K.; Cui, H.; Liu, J. Researches on corrosion behaviors of carbon steel/copper alloy couple under organic coating in static and flowing seawater. *Prog. Org. Coat.* **2022**, *166*, 106793. [CrossRef]
16. Wei, L.; Pang, X.; Gao, K. Effect of flow rate on localized corrosion of X70 steel in supercritical CO_2 environments. *Corros. Sci.* **2018**, *136*, 339–351. [CrossRef]
17. Robineau, M.; Romaine, A.; Sabot, R.; Jeannin, M.; Deydier, V.; Necib, S.; Refait, P. Galvanic corrosion of carbon steel in anoxic conditions at 80 °C associated with a heterogeneous magnetite (Fe_3O_4)/mackinawite (FeS) layer. *Electrochim. Acta* **2017**, *255*, 274–285. [CrossRef]
18. Ni, Q.; Xia, X.; Zhang, J.; Dai, N.; Fan, Y. Electrochemical and SVET Studies on the Typical Polarity Reversal of Cu–304 Stainless Steel Galvanic Couple in Cl−-Containing Solution with Different pH. *Electrochim. Acta* **2017**, *247*, 207–215. [CrossRef]
19. Choi, Y.-I.; Kuroda, K.; Okido, M. Temperature-dependent corrosion behaviour of flame-resistant, Ca-containing AZX911 and AMX602 Mg alloys. *Corros. Sci.* **2016**, *103*, 181–188. [CrossRef]
20. Sánchez-Tovar, R.; Montañés, M.; García-Antón, J. Contribution of the flowing conditions to the galvanic corrosion of the copper/AISI 316L coupling in highly concentrated LiBr solutions. *Corros. Sci.* **2013**, *68*, 91–100. [CrossRef]
21. Fang, X.; Fulin, Y.; Kun, L. Role of dissolved oxygen on the corrosion behavior of 316L stainless steel. *Mater. Des.* **2025**, *260*, 115017. [CrossRef]
22. Gao, K.; Yu, F.; Pang, X.; Zhang, G.; Qiao, L.; Chu, W.; Lu, M. Mechanical properties of CO_2 corrosion product scales and their relationship to corrosion rates. *Corros. Sci.* **2008**, *50*, 2796–2803. [CrossRef]
23. Nesic, S.; Wang, S.; Cai, J.; Xiao, Y. Integrated CO_2 corrosion-multiphase flow model. In Proceedings of the CORROSION 2004, New Orleans, LA, USA, 27 March–1 April 2004; pp. 1–26.
24. Zeng, H.; Yang, Y.; Zeng, M.; Li, M. Effect of dissolved oxygen on electrochemical corrosion behavior of 2205 duplex stainless steel in hot concentrated seawater. *J. Mater. Sci. Technol.* **2021**, *66*, 177–185. [CrossRef]
25. Han, B.; Ding, S.; Yu, X. Intrinsic self-sensing concrete and structures: A review. *Measurement* **2015**, *59*, 110–128. [CrossRef]
26. Wang, Q.; Qian, R.; Wang, Y.; Niu, W.; Wei, C. Microstructure and Stress Corrosion Behavior of Cold-Sprayed Al-Based Composite Coatings on Q345R Pressure Vessel Steel. *JOM* **2025**, *77*, 3576–3588. [CrossRef]
27. Fayomi, O. Achieving a super-strengthening functional composite coating from ZnO doped snail shell particulate for mitigation of mild steel towards improved microstructural, corrosion, and opto-electrical properties. *Results Surf. Interfaces* **2024**, *17*, 100294. [CrossRef]
28. Zellele, D.M.; Yar-Mukhamedova, G.S.; Rutkowska-Gorczyca, M. A Review on Properties of Electrodeposited Nickel Composite Coatings: Ni-Al_2O_3, Ni-SiC, Ni-ZrO_2, Ni-TiO_2 and Ni-WC. *Materials* **2024**, *17*, 5715. [CrossRef] [PubMed]
29. Dehghahi, S.; Amini, R.; Alizadeh, M. Corrosion, passivation and wear behaviors of electrodeposited Ni–Al_2O_3–SiC nano-composite coatings. *Surf. Coat. Technol.* **2016**, *304*, 502–511. [CrossRef]
30. Kumar, M.K.P.; Singh, M.P.; Srivastava, C. Electrochemical behavior of Zn–graphene composite coatings. *RSC Adv.* **2015**, *5*, 25603–25608. [CrossRef]
31. Berlia, R.; Kumar, M.K.P.; Srivastava, C. Electrochemical behavior of Sn–graphene composite coating. *RSC Adv.* **2015**, *5*, 71413–71418. [CrossRef]
32. Jasim, A.H.; Radhi, N.S.; Kareem, N.E.; Al-Khafaji, Z.S.; Falah, M. Identification and investigation of corrosion behavior of electroless composite coating on steel substrate. *Open Eng.* **2023**, *13*, 20220472. [CrossRef]
33. Kumar, R.; Mandal, S.K.; Saha, S.; Bishwakarma, H.; Kumar, R.; Singh, P.K. A study on the corrosion inhibition properties of nano MWCNTs on TMT steel rebar developed using electroless nickel phosphorous (Ni–P) coating. *Asian J. Civ. Eng.* **2024**, *25*, 4069–4079. [CrossRef]
34. Radhi, N.S.; Rasheed, F.S.; Al-Khafaji, Z.; Ali, K.O.; Ghazi, R. Improvement of Corrosion Resistance of Stainless Steel 316 by Electroless Phosphorus Nickel-Titania Composite Coating. *Corros. Sci. Technol.* **2025**, *24*, 51–62.
35. Jiang, B.; Wu, M.; Wu, S.; Ji, M. Study on anticorrosion of Q235 building steel using Iranian rock-graphene nanocomposite coating. *Alex. Eng. J.* **2023**, *71*, 73–77. [CrossRef]
36. Pandey, U.; Singh, A.; Sharma, C. Development of anti-corrosive novel nickel-graphene oxide-polypyrrole composite coatings on mild steel employing electrodeposition technique. *Synth. Met.* **2022**, *290*, 117135. [CrossRef]
37. Jyotheender, K.S.; Srivastava, C. Ni-graphene oxide composite coatings: Optimum graphene oxide for enhanced corrosion resistance. *Compos. Part B Eng.* **2019**, *175*, 107145. [CrossRef]
38. Selvam, M.; Saminathan, K.; Siva, P.; Saha, P.; Rajendran, V. Corrosion behavior of Mg/graphene composite in aqueous electrolyte. *Mater. Chem. Phys.* **2016**, *172*, 129–136. [CrossRef]
39. Rekha, M.; Kamboj, A.; Srivastava, C. Electrochemical behaviour of SnZn-graphene oxide composite coatings. *Thin Solid Films* **2017**, *636*, 593–601. [CrossRef]

40. Rashad, M.; Pan, F.; Asif, M.; Chen, X. Corrosion behavior of magnesium-graphene composites in sodium chloride solutions. *J. Magnes. Alloy.* **2017**, *5*, 271–276. [CrossRef]
41. Balandin, A.A.; Ghosh, S.; Bao, W.; Calizo, I.; Teweldebrhan, D.; Miao, F.; Lau, C.N. Superior Thermal Conductivity of Single-Layer Graphene. *Nano Lett.* **2008**, *8*, 902–907. [CrossRef] [PubMed]
42. Berry, V. Impermeability of graphene and its applications. *Carbon* **2013**, *62*, 1–10. [CrossRef]
43. Lee, C.; Wei, X.; Kysar, J.W.; Hone, J. Measurement of the elastic properties and intrinsic strength of monolayer graphene. *Science* **2008**, *321*, 385–388. [CrossRef] [PubMed]
44. Paredes, J.I.; Villar-Rodil, S.; Martínez-Alonso, A.; Tascón, J.M.D. Graphene Oxide Dispersions in Organic Solvents. *Langmuir* **2008**, *24*, 10560–10564. [CrossRef] [PubMed]
45. Dreyer, D.R.; Park, S.; Bielawski, C.W.; Ruoff, R.S. The chemistry of graphene oxide. *Chem. Soc. Rev.* **2010**, *39*, 228–240. [CrossRef] [PubMed]
46. Singh, S.; Samanta, S.; Das, A.K.; Sahoo, R.R. Tribological investigation of Ni-graphene oxide composite coating produced by pulsed electrodeposition. *Surf. Interfaces* **2018**, *12*, 61–70. [CrossRef]
47. Tseluikin, V.; Dzhumieva, A.; Yakovlev, A.; Mostovoy, A.; Zakirova, S.; Strilets, A.; Lopukhova, M. Electrodeposition and Corrosion Properties of Nickel–Graphene Oxide Composite Coatings. *Materials* **2021**, *14*, 5624. [CrossRef] [PubMed]
48. Dharanendra, R.a.; Shet Prakash, M.; Sekharappa, S.; Jagannath, K.V. Electrochemical Corrosion Behaviour of Nickel and Nickel-Reduced Graphene Oxide Coatings on Mild Steel in 3.5% NaCl Solution. *ECS Trans.* **2022**, *107*, 199–208. [CrossRef]
49. Tseluikin, V.; Dzhumieva, A.; Tikhonov, D.; Yakovlev, A.; Strilets, A.; Tribis, A.; Lopukhova, M. Pulsed Electrodeposition and Properties of Nickel-Based Composite Coatings Modified with Graphene Oxide. *Coatings* **2022**, *12*, 656. [CrossRef]
50. Wang, J.; Wu, D.; Zhu, C.; Xiang, Z. Thermal stability enhancement of hybrid Ni_2Al_3/Ni coatings on creep resistant ferritic steels by a mechanism of thermodynamically constrained interdiffusion. *Surf. Coat. Technol.* **2013**, *232*, 489–496. [CrossRef]
51. Yu, X.; Zhang, R.; Cui, G.; Li, Z. Influence of Pulse Parameters on the Morphology and Corrosion Resistance of Nickel-Graphene Composite Coating. *Int. J. Electrochem. Sci.* **2019**, *14*, 4754–4768. [CrossRef]
52. Ge, R.; Tang, J.; Li, W.; Liang, P. Electrodeposition of Cu Sn alloy coatings with enhanced corrosion resistance durability and self cleaning properties. *Sci. Rep.* **2025**, *15*, 14926. [CrossRef] [PubMed]
53. Staszuk, M.; Pakuła, D.; Reimann, Ł.; Woźniak, A.; Kloc-Ptaszna, A.; Kolasa, J.; Nuckowski, P. Investigations of CrN/TiO2 Coatings Obtained in the Hybrid PVD/ALD Process on 316L Steel Substrates. *Materials* **2026**, *19*, 1921. [CrossRef] [PubMed]
54. Pech-Núñez, D.; Gutiérrez, J.; Cruz, J.C.; Vega-Azamar, R.E.; Trejo-Arroyo, D.L.; Gurrola, M.P. Multi-walled carbon nanotubes—Zinc in commercial acrylic sealant as a coating for anticorrosive protection system in metallic building structures. *Eur. J. Environ. Civ. Eng.* **2023**, *27*, 4364–4378. [CrossRef]
55. Feng, Y.; Liu, M.; Jia, L.; Bai, Y.; Ma, G.; Zhou, X.; Wang, H.; Wang, H. Study on the Corrosion Resistance of Supersonic Plasma Spraying Al_2O_3 Thin Layer and SiO_2 Sealer Alternately Deposited Coating. *Coatings* **2024**, *14*, 78. [CrossRef]
56. Mehr, A.K.; Pourzadeh, D.; Mehr, A.K.; Farid-Shayegan, F.; Lotfi-Kaljahi, A.; Mizban, A.; Babaei, R. Development and characterization of corrosion-resistant plasma-sprayed Ni-Al composite coatings via graphene oxide fillers. *Ceram. Int.* **2024**, *50*, 55351–55362. [CrossRef]
57. Goswami, P.; Raman, R.K.S.; Alankar, A. Machine Learning Strategies to Circumvent Variabilities in Chemical Vapour-Deposited Graphene Coatings for Remarkable Corrosion Resistance of Metals. *Small Struct.* **2026**, *7*, e202500720. [CrossRef]
58. Prasanth, I.S.N.V.R.; Jeevanandam, P.; Selvaraju, P.; Sathish, K.; Ahammad, S.K.H.; Sujatha, P.; Kaarthik, M.; Mayakannan, S.; Sasikumar, B. Study of Friction and Wear Behavior of Graphene-Reinforced AA7075 Nanocomposites by Machine Learning. *J. Nanomater.* **2023**, *2023*, 5723730. [CrossRef]
59. Trentin, A.; Pakseresht, A.; Duran, A.; Castro, Y.; Galusek, D. Electrochemical Characterization of Polymeric Coatings for Corrosion Protection: A Review of Advances and Perspectives. *Polymers* **2022**, *14*, 2306. [CrossRef] [PubMed]
60. Lillard, R.S.; Moran, P.J.; Isaacs, H.S. A Novel Method for Generating Quantitative Local Electrochemical Impedance Spectroscopy. *J. Electrochem. Soc.* **1992**, *139*, 1007–1012. [CrossRef]
61. Loveday, D.; Peterson, P.; Rodgers, B. Evaluation of organic oatings with electrochemical impedance spectroscopy. Part 2: Application of EIS to coatings. *JCT Coatingstech* **2004**, *1*, 88–93.
62. Frias-Cacho, X.; Castro, M.; Nguyen, D.-D.; Grolleau, A.-M.; Feller, J.-F. A Review of In-Service Coating Health Monitoring Technologies: Towards "Smart" Neural-Like Networks for Condition-Based Preventive Maintenance. *Coatings* **2022**, *12*, 565. [CrossRef]
63. Bierwagen, G.; Tallman, D.; Li, J.; He, L.; Jeffcoate, C. EIS studies of coated metals in accelerated exposure. *Prog. Org. Coat.* **2003**, *46*, 149–158. [CrossRef]
64. Grossi, M.; Riccò, B. Electrical impedance spectroscopy (EIS) for biological analysis and food characterization: A review. *J. Sens. Sens. Syst.* **2017**, *6*, 303–325. [CrossRef]
65. Zubielewicz, M.; Gnot, W. Mechanisms of non-toxic anticorrosive pigments in organic waterborne coatings. *Prog. Org. Coat.* **2004**, *49*, 358–371. [CrossRef]

66. Attar, M.M. Investigation on zinc phosphate effectiveness at different pigment volume concentrations via electrochemical impedance spectroscopy. *Electrochim. Acta* **2005**, *50*, 4645–4648. [CrossRef]
67. Obot, I.; Onyeachu, I.B. Electrochemical frequency modulation (EFM) technique: Theory and recent practical applications in corrosion research. *J. Mol. Liq.* **2018**, *249*, 83–96. [CrossRef]
68. Mahdavian, M.; Attar, M. Another approach in analysis of paint coatings with EIS measurement: Phase angle at high frequencies. *Corros. Sci.* **2006**, *48*, 4152–4157. [CrossRef]
69. Mousavifard, S.; Attar, M.; Ghanbari, A.; Dadgar, M. Application of artificial neural network and adaptive neuro-fuzzy inference system to investigate corrosion rate of zirconium-based nano-ceramic layer on galvanized steel in 3.5% NaCl solution. *J. Alloy. Compd.* **2015**, *639*, 315–324. [CrossRef]
70. Wang, C.; Li, W.; Wang, Y.; Yang, X.; Xu, S. Study of electrochemical corrosion on Q235A steel under stray current excitation using combined analysis by electrochemical impedance spectroscopy and artificial neural network. *Constr. Build. Mater.* **2020**, *247*, 118562. [CrossRef]
71. Kubisztal, J.; Kubisztal, M.; Haneczok, G. Corrosion damage of 316L steel surface examined using statistical methods and artificial neural network. *Mater. Corros.* **2020**, *71*, 1842–1855. [CrossRef]
72. Zeraati, M.; Abbasi, H.; Ghaffarzadeh, P.; Chauhan, N.P.S.; Sargazi, G. Application of Artificial Neural Networks for Corrosion Behavior of Ni–Zn Electrophosphate Coating on Galvanized Steel and Gene Expression Programming Models. *Front. Mater.* **2022**, *9*, 823155. [CrossRef]
73. Jiang, F.; Hirohata, M. A deep learning-based corrosion prediction model for paint-coated steel with defects. In *Life-Cycle of Structures and Infrastructure Systems*, 1st ed.; CRC Press: London, UK, 2023; pp. 631–638.
74. Radhika, N.; Sabarinathan, M.; Sivaraman, S. A Comparative Analysis of Machine Learning Techniques for Predicting the Wear Rate of Ceramic Coated Steel. *IEEE Access* **2024**, *12*, 146949–146967. [CrossRef]
75. Oliveira, L.M.D.; Silva, F.L.D.; Janissek, P.R.; Toniolo, J.C. Technological Advances in Electroplating: Artificial Intelligence to Predict Zinc Coating Thickness on SAE 1008 Low Carbon Steels. *Quím. Nova* **2025**, *48*, e-20250103.
76. Radhika, N.; Sabarinathan, M.; Sivaraman, S. Utilization of Ensemble Techniques in Machine Learning to Predict the Porosity and Hardness of Plasma-Sprayed Ceramic Coating. *IEEE Access* **2025**, *13*, 136160–136174. [CrossRef]
77. Liu, L.; Li, R.; Ye, D.; Yao, J. Prediction of Porosity in Atmospheric Plasma Sprayed Thermal Barrier Coatings Using Terahertz Pulse and Hybrid Machine Learning Algorithms. In Proceedings of the 3rd Asia Pacific Conference on Plasma and Terahertz Science (APCOPTS), Busan, Republic of Korea, 25–28 August 2023; pp. 5104–5111.
78. Tran, N.-L.; Nguyen, T.-H.; Phan, V.-T.; Nguyen, D.-D. A Machine Learning-Based Model for Predicting Atmospheric Corrosion Rate of Carbon Steel. *Adv. Mater. Sci. Eng.* **2021**, *2021*, 6967550. [CrossRef]
79. Kosari Mehr, A.; Kosari Mehr, A.; Pourzadeh, D.; Babaei, R.; Lotfi-Kaljahi, A.; Mizban, A.; Fa-rid-Shayegan, F. Corrosion-resistant plasma-sprayed Ni-Al composite coatings using graphene oxide fillers. *MenDeley Data* **2024**, *V1*. [CrossRef]
80. Cosut, M.; Bekdas, G.; Nigdeli, S.M.; Isikdag, U. Predicting design suitability of box-shaped sustainable timber structural members using machine learning and hyperparameter optimization. *Neural Comput. Appl.* **2025**, *37*, 24123–24148. [CrossRef]
81. Breiman, L. Random forests. *Mach. Learn.* **2001**, *45*, 5–32. [CrossRef]
82. Gron, A. Chapter 7: Ensemble Learning and Random Forests. In *Hands-On Machine Learning with Scikit Learn Keras Tensorflow*, 3rd ed.; Oreilly: Sebastopol, CA, USA, 2019; p. 220.
83. Chicco, D.; Warrens, M.J.; Jurman, G. The coefficient of determination R-squared is more informative than SMAPE, MAE, MAPE, MSE and RMSE in regression analysis evaluation. *PeerJ Comput. Sci.* **2021**, *7*, e623. [CrossRef] [PubMed]
84. Scikit-Learn Developers. 3.4.6. Regression Metrics. In Metrics and Scoring: Quantifying the Quality of Predictions. Scikit-Learn. Available online: https://scikit-learn.org/dev/modules/model_evaluation.html#regression-metrics.n (accessed on 25 June 2026).
85. Geisser, S.; Eddy, W.F. A predictive approach to model selection. *J. Am. Stat. Assoc.* **1979**, *7*, 153–160. [CrossRef]
86. Zhang, W.; Wu, C.; Li, Y.; Wang, L.; Samui, P. Assessment of pile drivability using random forest regression and multivariate adaptive regression splines. *Georisk Assess. Manag. Risk Eng. Syst. Geohazards* **2019**, *15*, 27–40. [CrossRef]
87. Ocak, A.; Kahvecioğlu, B.; Nigdeli, S.M.; Bekdaş, G.; Işıkdağ, Ü.; Geem, Z.W. Machine Learning-Based Prediction of Operability for Friction Pendulum Isolators Under Seismic Design Levels. *Big Data Cogn. Comput.* **2026**, *10*, 29. [CrossRef]
88. Schader, L.M.; Song, W.; Kempker, R.; Benkeser, D. Don't Let Your Analysis Go to Seed: On the Impact of Random Seed on Machine Learning-based Causal Inference. *Epidemiology* **2024**, *35*, 764–778. [CrossRef] [PubMed]